INORGANIC CHEMISTRY
FRONTIERS

REVIEW

View Article Online
View Journal | View Issue

Cite this: *Inorg. Chem. Front.*, 2022, **9**, 6330

Array configurations of oxometallate–Ag cluster hybrid nanocomposites

Jia-Qi Wang,*†[a,b] Min-Hong Yan,†[a] Shengchang Xiang,[a] Xi Fan*[a,b] and Zhangjing Zhang*[a]

Received 19th September 2022,
Accepted 18th October 2022

DOI: 10.1039/d2qi02002e

rsc.li/frontiers-inorganic

Oxometallate (MO)-modified Ag clusters have attracted considerable research interest due to their aesthetic structures and fascinating properties. MOs can be a key factor in the organization of Ag ions into a complex entity in an ordered way. Enormous effort has been devoted to exploiting the synthetic strategy of MO–Ag cluster hybrid nanocomposites. Herein, we intend to review the recent progress in the design and construction of MO–Ag clusters with daedal architectures and potential applications. Accordingly, six different types of MO–Ag clusters are summarized mainly in terms of array configurations: (1) MOs @ Ag shells; (2) Ag core @ MOs; (3) Ag core @ MOs @Ag shells; (4) coordination polymers; (5) intercluster compounds and (6) mixed array configurations. Besides, the synergistic effects between MOs and Ag clusters are presented. Based on the current development in this area, this minireview is expected to provide a perspective on controllable preparation of MO–Ag clusters, and a basic understanding of the structure/property correlations of Ag nanoparticle-metal oxide materials, thereby assisting in building functional nanomaterials.

1. Introduction

Controllable synthesis of metal nanocomposites is a forefront research topic in the field of metal nanoparticles. Among them, silver-transition metal oxide composites show unique physicochemical properties and potential catalytic activity, due to the interfacial effects.[1–4] However, it is still a daunting challenge to investigate the metal nanoparticle/support interfacial interactions due to the lack of real molecular models. To overcome these intrinsic drawbacks, atomically precise Ag clusters and oxometallates (MOs) are employed as building units to construct hybrid assemblies. Compared with traditional Ag nanoparticles, Ag clusters have exhibited a variety of advantages in catalytic properties,[5–7] such as quantum size effects, definite atomic arrangements and unique surface structures. MOs are molecular oxides based on high-valence early transition metals, which can be regarded as model compounds of transition metal oxides. According to the classic hard and soft acids and bases (HSAB) theory, Ag atoms as a soft acid would be preferable for soft-base organic ligands like phosphines, thiolates and alkynyls, but have a weaker tendency for inorganic oxo anions. However, the multiple negative valence states of MOs can assist in the effective charge balance of Ag cluster cations. Additionally, compared with commonly used organic molecules serving as terminal or bridging ligands on the surface of the cluster cores, MOs possess multiple oxygen atoms, leading to many more various interfacial bonding configurations and assembly modes. Therefore, despite the presence of HSABs, MOs can act as a substrate and co-assemble with Ag species effectively. Plenty of MO–Ag cluster hybrid composites have been extensively designed with novel physical/chemical properties and potential applications in the fields of optics, electricity, catalysis, *etc.*[8–10] There are several unique advantages of MO–Ag cluster hybrid composites (Scheme 1): (1) novel and various coordination motifs between MOs and Ag atoms can enrich the structural diversity of hybrid clusters; (2) MOs can participate in the frontier orbitals of Ag clusters and contribute to the electronic structure, endowing them with unique functionalities; (3) Ag cluster–MO hybrid composites serve as a molecular model for silver nanoparticle/metal oxide materials to advance the fundamental study in nanoscience and nanotechnology. However, one question always made researchers confused as to what specific role do MOs play in the construction of hybrid nanocomposites. Therefore, it is essential to categorize these MO–Ag clusters based on their assembly modes.

So far, some reviews on MO-based Ag clusters have been published. For instance, Wang's group summarized the structures and properties of anion-templated silver clusters.[8]

[a]*Fujian Provincial Key Laboratory of Polymer Materials, College of Chemistry and Materials Science, Fujian Normal University, Fuzhou, Fujian 350007, PR China. E-mail: wangjq@fjnu.edu.cn, fanxi@fjnu.edu.cn, zzhang@fjnu.edu.cn*
[b]*State Key Laboratory of Structural Chemistry, Fujian Institute of Research on the Structure of Matter, Chinese Academy of Sciences, Fuzhou, Fujian 350002, PR China*
†These authors contributed equally to this review.

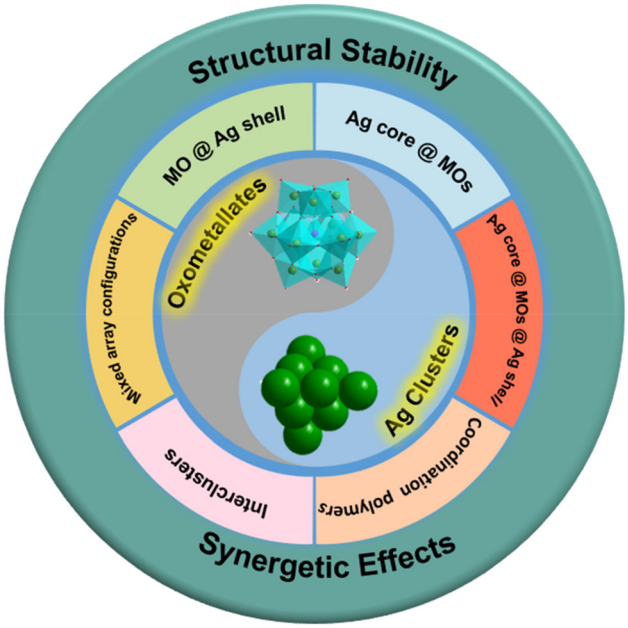

Scheme 1 The schematic diagram of the assembly modes which are classified into six types, including MO @ Ag shells, Ag core @ MOs, Ag core @ MOs @ Ag shells, coordination polymers, intercluster compounds and mixed array configurations.

Recently, Zheng and his partners published an elaborate review on POM-templated high-nuclear Ag clusters.[9] Moreover, Zhang and his co-workers published a review focusing on Ag clusters protected by oxometallates.[10] These reviews reveal that the arrangements of nanosized silver clusters and MO anions in the crystal structure can account for their synergistic effects. However, there is no comprehensive review summarizing the arrangements of structural configurations in various Ag–MO systems. Therefore, a review focusing on the categories of MO roles in the synthesis of MO-based Ag clusters will assist in understanding the structure–property and structure–functionality correlations. In this review, the assembly modes of Ag cluster–MO hybrid nanocomposites are introduced and the specific contribution of MOs to the construction of hybrid nanostructures is emphatically summarized. Meanwhile, we focused on the decisive effect of MOs on the physicochemical properties of silver clusters. Moreover, some insights into structure–effect relationships will be put forward, in terms of improving the rational design of such nanocomposites with potential applications.

2. The assembly modes of MO–Ag cluster hybrid nanocomposites

Ag clusters modified by metal-oxo module engineering have demonstrated significant effectiveness and potential in recent years. Therein, the geometric symmetry and charge distribution of MOs can influence the assembly process of hybrid clusters, and thus induce the interaction mode of MOs and Ag clusters. According to their structural characteristics, the Ag cluster–MO nanocomposites are basically classified into five categories in Fig. 1: (1) MO @ Ag shells; (2) Ag core @ MOs; (3) Ag core @ MOs @ Ag shells; (4) coordination polymers; and (5) intercluster compounds. Actually, the combination of any two kinds of cluster composites mentioned above can give rise to (6) mixed array configurations, which greatly stimulate the expansion of structural diversity in this field.

2.1. MO @ Ag shell mode

Metal-oxo modules are widely employed in an anion templating approach. The cluster nuclearity and shape can be controlled by adjusting the size and geometry of metal-oxo modules. Hence, the reported MO @ silver(I) clusters are classified into the following three subclasses based on the types of MOs: (1) mononuclear oxometallates @ Ag clusters; (2) isopolyoxoanions @ Ag clusters; and (3) heteropolyoxoanions @ Ag clusters.

2.1.1. Mononuclear oxometallates @ Ag clusters. The arrangement of multiple mononuclear oxometallates within silver nanoclusters can tailor skeleton shapes to spheres, anisotropic oblate spheroids or elongated rods. Tetrahedral anions such as CrO_4^{2-} are chosen to induce the generation of spherical Ag cages.[11] In 2009, Wang's group used CrO_4^{2-} as the directing agent to prepare $[CrO_4@Ag_{22}(C{\equiv}C^tBu)_{18}](BF_4)_2$. The shortest Ag–O distance is 2.634 Å, indicating that CrO_4^{2-} binds loosely with the Ag(I) cage.[12] By using flat PhC≡C– in place of the bulky ^{t}BuC≡C ligand, a new peanut-shaped $[Ag_{35}(C{\equiv}CPh)_{28}(CrO_4)_2(TMEDA)_4]^{3+}$ cluster was isolated.[12] The double-chromate templated $[(CrO_4)_2@Ag_{35}]$ kernel can be viewed as the fusion of two single cages of $CrO_4@Ag_{22}$ with five shared silver atoms. Su's group isolated a multi-shell silver cluster $[Ag_{55}(MoO_4)_6(C{\equiv}C^tBu)_{24}(CH_3COO)_{18}]^+$ having a six-fold symmetry, which is templated by six $[MoO_4]^{2-}$ anions.[13] Besides silver–alkynyl clusters, the chromate-templating effect on silver–sulfide clusters also deserves to be explored. The reaction of $\{(HNEt_3)_2[Ag_{10}(SC_6H_4{}^tBu)_{12}]\}_n$ with CF_3COOAg and $K_2Cr_2O_7$ yielded tetrahedral $[Ag(CrO_4)_4@Ag_{46}(SC_6H_4{}^tBu)_{24}(CF_3COO)_{18}(DMF)_4]^{3-}$,[14] whose shell consists of a silver-

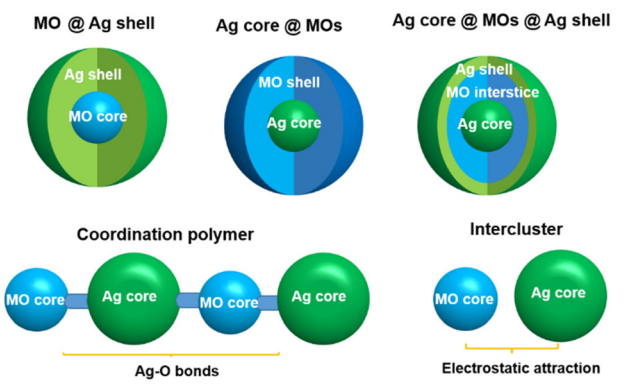

Fig. 1 Illustration of five array configurations of the MO–silver cluster kernel.

centred Ag_{11} superadamantane capped by four half-cuboctahedra, wrapping four templating CrO_4^{2-}. In addition to CrO_4^{2-}, MoO_4^{2-} is a tetrahedral oxyanion and widely used in directing the formation of nanosized Ag cages.[15] Sun's group obtained $[Ag_4(MoO_4S_4)_5$ @$Ag_{66}(^tBuC_6H_4S)_{40}(mbc)_{15}(H_2O)_2]^{3-}$ by the reaction of Ag_2O, Na_2MoO_4, and *m*-methoxybenzoic acid in CH_3OH/CH_2Cl_2, and found that the outer S_4 square is associated with the inner $[(MoO_4)@Ag_4(MoO_4)_4]$ square array.[16] They also reported $[(MoO_4)_5@Ag_{52}S_6(^tBuC_6H_4S)_{20}(dppm)_{10}@(MoO_4)_{10}]^{10-}$ with the shape of an anisotropic oblate spheroid, involving templating of five MoO_4^{2-} ions.[17] The above cases indicate that the arrangement of multiple tetrahedral anions inside Ag cages can control the size and shape of cluster products, as shown in Fig. 2.

2.1.2. Isopolyoxoanions @ Ag clusters. Polyoxometalates (POMs) are a class of metal-oxo clusters with structural versatility. Thus, the strategy of encapsulation of POMs into silver cages gives rise to a series of fascinating structures. Among them, isopolyoxoanions containing only one kind of early transition metal ion are important family members of POMs and widely employed in directing Ag ions to gather into high-nuclear clusters of variable geometric structures.

Isopolyoxoanions usually isomerize or transform to other forms different from their original compositions and structures when enwrapped into the silver cages. The precursor $[Mo_7O_{24}]^{6-}$ is labile and can be transformed into two $[Mo_6O_{22}]^{8-}$ configurations with higher charge densities. $[(A\text{-}Mo_6O_{22})_2@Ag_{60}(^tBuC{\equiv}C)_{38}](OTf)_6$ was prepared through the reaction of $[^tBuC{\equiv}CAg]_n$ with AgOTf followed by the addition of $[Mo_7O_{24}]^{6-}$.[18] The cluster skeleton can be viewed as two $[Mo_6O_{22}]^{8-}$ nuts encapsulated within peanut shell-like Ag_{60}. The reaction of the precursor $[Mo_7O_{24}]^{6-}$ with $AgCF_3COO$ and $\{(HNEt_3)_2[Ag_{10}(SC_6H_4{}^tBu)_{12}]\}_n$ gave rise to a mango-like $B\text{-}Mo_6O_{22}@Ag_{58}S_2(SC_6H_4{}^tBu)_{36}(CF_3COO)_{10}$ cluster,[19] which can be viewed as two $Ag_{10}S_6$ bowls capped upside and downside of a $Ag_{38}S_{26}$ belt in Fig. 3a.

The enclosure of the $[A\text{-}Mo_6O_{22}]^{8-}$ anion can also be found in C_{2h}-symmetry $Mo_6O_{22}@Ag_{40}(^tBuC{\equiv}C)_{20}(CF_3COO)_{12}$ with Lindqvist-type $[Mo_6O_{19}]^{2-}$ as the POM precursor.[20] As we know, there are only 6 terminal oxygen atoms in the classical Lindqvist-type anion, whereas $[Mo_6O_{22}]^{8-}$ possesses 16 terminal oxygen atoms, improving its template effect. In addition to the silver–alkynyl clusters above, the $[Mo_6O_{19}]^{2-}$ polyoxoanion can undergo a reassembly for changing the nuclearity in the formation of POM-based silver thiolate nanoclusters.[21] Gao *et al.* isolated a giant peanut-like $[(Mo_{20}O_{66})@Ag_{62}(S^tBu)_{40}]^{10+}$ cluster, comprising the Ag_{62} shell and $[Mo_{20}O_{66}]^{12-}$ polyoxoanion core generated from $[Mo_6O_{19}]^{2-}$.[22] *In situ* generated $[\alpha\text{-}Mo_5O_{18}]^{6-}$ from $(^nBu_4N)_2[Mo_6O_{19}]$ can be captured in the interior of the shuttle-shaped $Ag_{38}(^tBuS)_{18}(PhCOO)_{14}$ shell (Fig. 3b).[15] $[(W_6O_{21})@Ag_{34}(^tBuS)_{26}(CF_3COO)]^+$ was obtained from the reaction of ^tBuSAg, CF_3COOH, $(Bu_4N)_2[W_6O_{19}]$ and Et_3N in methanol,[23] whose central anion $[W_6O_{21}]^{6-}$ originated from the isomerization of the $[W_6O_{19}]^{2-}$ precursor.

In addition to Lindqvist-type POMs, $[\alpha\text{-}Mo_8O_{26}]^{4-}$ is widely employed as a POM percursor to direct Ag ions to aggregate into high-nuclear clusters. However, $[\alpha\text{-}Mo_8O_{26}]^{4-}$ is easily decomposed into $[MoO_4]^{2-}$.[13] In 2018, Sun's group realized the isolation of $Mo_7O_{24}@Ag_{41}(^iPrS)_{19}(p\text{-}TOS)_{16}(CH_3OH)_4$ and $Mo_5O_{18}@Ag_{36}(^iPrS)_{18}(PhSO_3)_{12}(DMF)_6$.[24,25] With such a synthetic method, they reported $[(Mo_8O_{28})@Ag_{48}(p\text{-}MePhS)_{24}(CF_3COO)_{14}(H_2O)_4(DMF)_2]^{2+}$ encapsulating unprecedented $[Mo_8O_{28}]^{8-}$, which is generated from $[\alpha\text{-}Mo_8O_{26}]^{4-}$ (Fig. 3c).[26] These examples further confirm that the POM precursors tend to transform into the corresponding templates with higher negative charge densities, more terminal oxygen atoms and stronger coordination ability to Ag atoms, which promotes the stabilization of the core–shell configuration. However, the flexible polyoxoanion templates often lead to unpredictable structures.

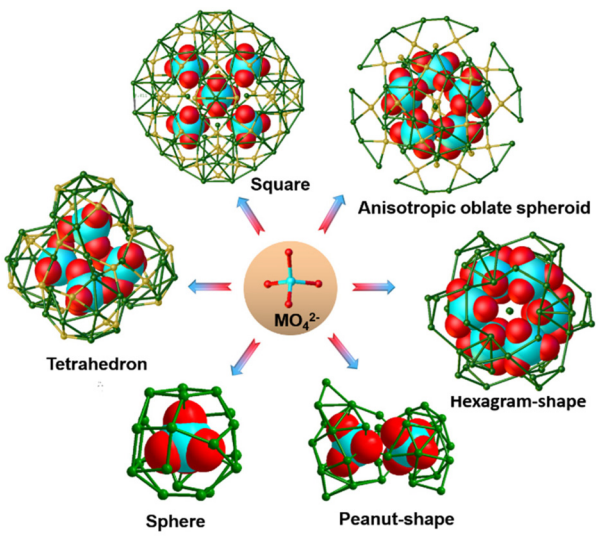

Fig. 2 Illustration of the inductive effect of mononuclear oxometallates on the nuclearity and geometry of the Ag cages (M = Cr/Mo).

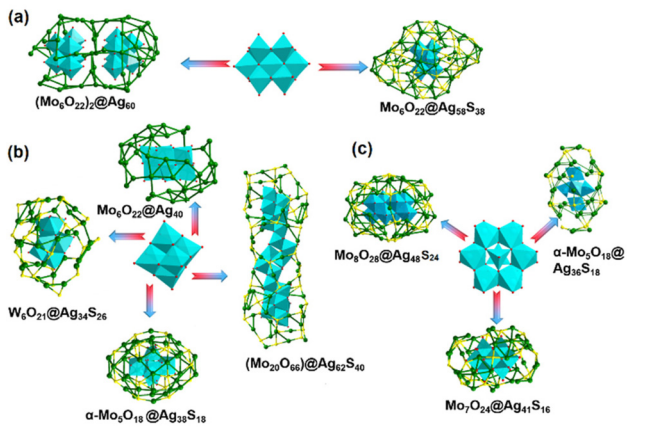

Fig. 3 A summary of the transformation of POMs in the reported Ag clusters: (a) $[Mo_7O_{24}]^{6-}$ precursor, (b) Lindqist-type precursor and (c) $[\alpha\text{-}Mo_8O_{26}]^{4-}$precursor. The C and H atoms are omitted for clarity.

Given the fact that the synthesis of POM-templated Ag clusters always relies on luck, researchers are seeking an approach to control the silver cluster structures at the molecular level. Apart from the serendipitous transformation cases mentioned above, it is notable that some specific stimuli can trigger the structural transformation of POM-based Ag clusters. Gao *et al.* used polyoxovanadate as the template anion to construct dodecahedrane-like $[Ag_{30}(^{t}BuS)_{20}V^{V}_{10}V^{IV}_{2}O_{34}]$,[27] and found that the thiolate Ag cluster can respond to external acid–base stimuli. With its Ag nanosized cage intact, the polyoxovanadate core undergoes transformation to a D_{3d} configuration upon acidification, and reverts to its original C_{2h} structure upon addition of a base (Fig. 4a). As shown in Fig. 4b, Sun *et al.* found that PhCOOH can induce the synergetic core–shell transformation involving enlargements of the inner anion template ($Mo_6O_{22}^{8-} \rightarrow Mo_8O_{28}^{8-}$) and the external silver(I) thiolate cage $(Ag_{44}(^{i}PrS)_{20}(PhCOO)_{16}(CH_3CN)_2 \rightarrow Ag_{50}(^{i}PrS)_{24}(PhCOO)_{18}(CH_3CN)_2)$. This is the first example of a smaller-to-larger silver nanocluster conversion *via* anion template growth. The proposed breakage–growth–reassembly mechanism based on time-dependent ESI-MS can provide inspiration for the design of new POM/organosilver(I) functional materials.[28]

Some flexible isopolyoxoanions can undergo structural transformation into new forms adapting to the peripheral silver cage, while some isopolyoxoanions retain their original compositions and structures when participating in the formation of silver clusters. In the presence of CF_3COOH in an organic medium, the reaction of $[^{t}BuC{\equiv}CAg]_n$, CF_3COOAg and $[H_3V_{10}O_{28}]^{3-}$ gave rise to $V_{10}O_{28}@Ag_{40}(^{t}BuC{\equiv}C)_{22}(CF_3COO)_{12}$ with C_{2h} symmetry.[20] The ellipsoidal skeleton consists of 40 silver atoms and $[V_{10}O_{28}]^{6-}$. The acidic conditions can limit the decomposition of $[V_{10}O_{28}]^{6-}$ anions into low-nuclearity species, but under basic conditions, $[V_{10}O_{28}]^{6-}$ decomposes readily into $[V_2O_7]^{4-}$, immediately. Although the same silver salt, $[^{t}BuC{\equiv}CAg]_n$ and polyoxometalate salts were employed as the reactants, $V_2O_7@Ag_{24}(C{\equiv}C^{t}Bu)_{14}(CF_3COO)_6$ was isolated with a smaller oxoanion inside the smaller Ag cage (Fig. 4c). Thus, the presence of acid/base sources may be an important factor to the transformation of isopolyoxoanions during the formation of POM-encapsulated silver clusters.

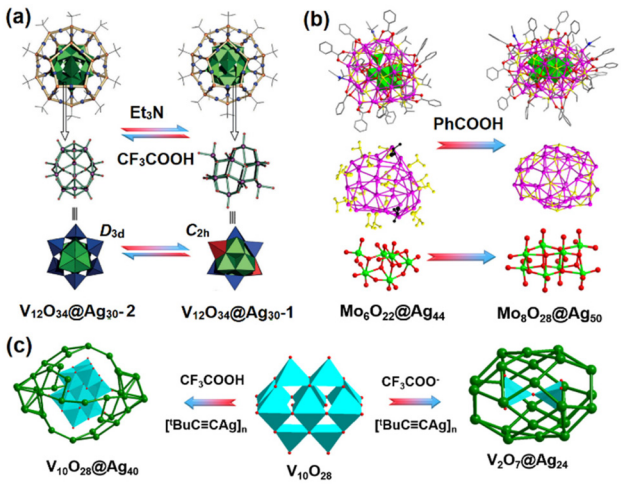

Fig. 4 (a) The transformation of polyoxovanadate cores inside the $[Ag_{30}(^{t}BuS)_{20}]^{10+}$ shell. Reproduced with permission from ref. 27. Copyright 2016 Wiley-VCH. (b) Core–shell transformation from **$Mo_6O_{22}@Ag_{44}$** to **$Mo_8O_{28}@Ag_{50}$**. Reproduced with permission from ref. 28. Copyright 2018, Nature Publishing Group. (c) The synthesis of **$V_2O_7@Ag_{24}$** and **$V_{10}O_{28}@Ag_{40}$** using the $[V_{10}O_{28}]^{6-}$ precursor under basic and acidic conditions.

2.1.3. Heteropolyoxoanions @ Ag clusters. Different from isopolyoxoanions, heteropolyoxoanions are POMs formed from the fusion of different inorganic oxygenates, and its designable synthesis and controllable properties *via* heteroatom doping are advantageous in catalysis, electrochemistry, *etc.*[29] Hence, the introduction of heteropolyoxoanions into Ag cluster systems can influence the function of the final products through bringing in their intrinsic properties.

Keggin-structured heteropolyoxoanions as templates. In 2014, Wang *et al.* synthesized a silver alkynyl cluster, namely, $[(PW_9O_{34})_2@Ag_{70}(^{t}BuC{\equiv}C)_{44}(H_2O)_2]^{8+}$ containing a Ag_{70} shell and two lacunary $[PW_9O_{34}]^{9-}$ templating ions by an ionothermal approach.[30] Ten Ag(I) ions are accommodated in the middle of the skeleton and sandwiched by the $[PW_9O_{34}]^{9-}$ units. As shown in Fig. 5a, cyclic voltammetric studies on $[BMIm]BF_4$ (BMIm = 1-butyl-3-methylimidazolium) reveal that there is fast core–shell electronic communication between the

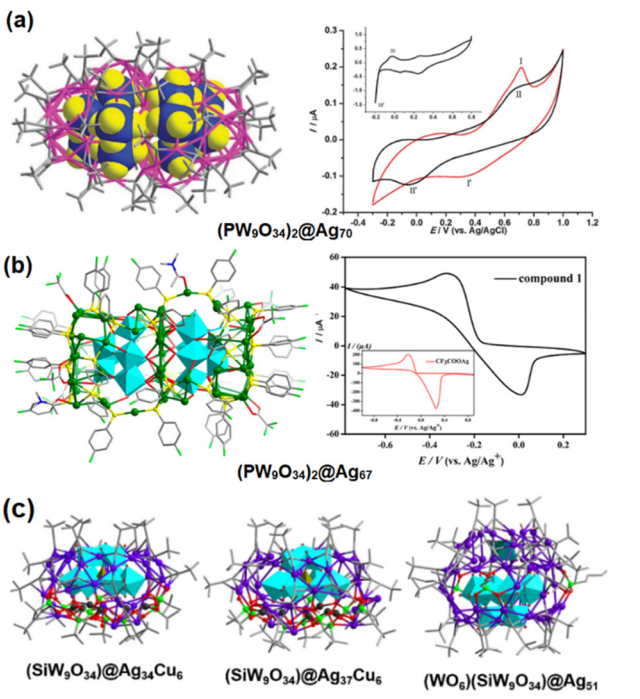

Fig. 5 (a) Molecular structure (left) and cyclic voltammogram (right) of **$(PW_9O_{34})_2@Ag_{70}$**. Reproduced with permission from ref. 30. Copyright 2012, Royal Society of Chemistry. (b) Molecular structure (left) and cyclic voltammogram (right) of **$(PW_9O_{34})_2@Ag_{67}$**. Reproduced with permission from ref. 31. Copyright 2018 American Chemical Society. (c) Molecular structures of **$(SiW_9O_{34})@Ag_{34}Cu_6$**, **$(SiW_9O_{34})@Ag_{37}Cu_6$** and **$(WO_6)(SiW_9O_{34})@Ag_{51}$**. Reproduced with permission from ref. 32. Copyright 2018, Wiley-VCH.

inner $[PW_9O_{34}]^{9-}$ and outer Ag ions. Using the same POMs, Zang's group prepared $[(PW_9O_{34})_2@Ag_{67}(p\text{-F PhS})_{36}(DMAc)_2(CF_3COO)_6]\cdot(CF_3COO)_7$ (**$(PW_9O_{34})_2@Ag_{67}$**). For this silver thiolate nanocluster, the separator is an almost flat plane of Ag_{12}, which is sandwiched by two lacunary Keggin phosphotungstate anions.[31] The difference in the redox behavior between the CF_3COOAg precursor and **$(PW_9O_{34})_2@Ag_{67}$** can be observed in Fig. 5b, affected by the central $[PW_9O_{34}]^{9-}$. Xie and his partners succeeded in isolating three $[SiW_9O_{34}]^{10-}$-templated clusters, $[(SiW_9O_{34})@Ag_{34}Cu_6(^t\text{BuC}{\equiv}\text{C})_{18}(^t\text{BuPO}_3)_9(CH_3CN)_2(H_2O)]$, $[(SiW_9O_{34})@Ag_{37}Cu_6(^t\text{BuC}{\equiv}\text{C})_{18}(^t\text{BuPO}_3)_9(CH_3CN)_6]^{2+}$, and $[(WO_6)(SiW_9O_{34})@Ag_{51}(^t\text{BuC}{\equiv}\text{C})_{27}(^n\text{BuPO}_3)_3(CH_3CO_2)_3(CH_3CN)_3]^{2-}$ (Fig. 5c).[32] Such an observation indicates that Ag clusters with various structures can be successfully constructed through the same POM template.

Although there have been various reports on the design and synthesis of Keggin-heteropolyacid @ silver clusters, the high-dimensional assembly in this field is still rare. Sun's group achieved face-fusion transformation from single-pod pumpkin-like $[(PW_9O_{34})@Ag_{51}(^i\text{PrS})_{25}(CF_3COO)_{17}(DMF)_3(CH_3OH)_3]$ (**$PW_9O_{34}@Ag_{51}$**) to double-pod **$(PW_9O_{34})_2@Ag_{72}$** by modifying the Ag shell with bridging ligands, which replaced the coordinated DMF ligands and constructed a POM@Ag cluster-based MOF.[33] As illustrated in Fig. 6, the introduction of 4,4′-bipyridine (bipy) and 1,4-bis(4-pyridinylmethyl)piperazine (pi-bipy) into **$PW_9O_{34}@Ag_{51}$** induces the assembly of a 2D 4^4-*sql* layered $\{[(PW_9O_{34})_2@Ag_{72}S(^i\text{PrS})_{41}(CF_3COO)_8(\text{bipy})_{5.5}(CH_3OH)(H_2O)]CF_3COO\}_n$ and a 3*D pcu* framework $\{[(PW_9O_{34})_2@Ag_{72}S(^i\text{PrS})_{42}(CF_3COO)_7(\text{pi-bipy})_{4.5}(CH_3OH)]_3CF_3COO\}_n$, respectively. The proposed breakage–fusion conversion is similar to the transformation from **$Mo_6O_{22}@Ag_{44}$** to **$Mo_8O_{28}@Ag_{50}$**.[28] Notably, the major differences appear in the Ag ligand shells, while $[PW_9O_{34}]^{9-}$ remains intact during the cluster transformation and cluster-based network formation, which is distinguished from the templating-anion-conversed cases mentioned in the 2.1.2 section. The new exploration gives a probable strategy to simultaneously induce structural transformation with the POM core intact and the high-dimensional assembly of POM @ Ag *via* employing bridging ligands.

Waugh-structured heteropolyoxoanions as templates. Wang *et al.* synthesized a 64-nuclearity silver alkynyl cluster, namely, $Mn^{III}Mn^{IV}{}_2Mo_{14}O_{56}@Ag_{64}(C{\equiv}C^t\text{Bu})_{38}(CF_3COO)_8$ (**$Mn^{III}Mn^{IV}{}_2Mo_{14}O_{56}@Ag_{64}$**).[34] As shown in Fig. 7b, a *meso* POM anion $[Mn^{III}Mn^{IV}{}_2Mo_{14}O_{56}]^{17-}$ is constructed by using the Waugh-type racemic-$\{Mn^{IV}Mo_7\}$ units connected together through a $\{Mn^{III}\}$ fragment. Furthermore, the ESR studies confirmed the existence of a mixed valence of Mn(III) and Mn(IV), and the comparison of voltammetric behaviors between **$Mn^{III}Mn^{IV}{}_2Mo_{14}O_{56}@Ag_{64}$** and $[MnMo_9O_{32}]^{6-}$ can reveal that the outer silver shell also participates in the redox process (Fig. 7c and d).

Weakley-structured heteropolyoxoanions as templates. Zuo *et al.* obtained $[HoW_{10}O_{36}@Ag_{42}(^t\text{BuC}{\equiv}\text{C})_{28}Cl_4]^+$ (**$HoW_{10}O_{36}@Ag_{42}$**), which has a peanut-like skeleton with $HoW_{10}O_{36}$ as the nuts and 42 silver(I) ions constructing the shell (Fig. 8a). The magnetic measurements reveal that **$HoW_{10}O_{36}@Ag_{42}$** shows a similar SMM (single-molecule magnetic) behaviour to the free parent cluster $[HoW_{10}O_{36}]^{9-}$, which arises from the Ho(III) ion (Fig. 8b and c).[35] The encapsulation *via* silver cages can be an effective means to separate the single SMM molecules from each other and achieve magnetic insulation. Another functional Weakley-POM can also endow the cluster composites with special physicochemical properties. Sun and coworkers employed the red-emissive Weakley-type $[EuW_{10}O_{36}]^{9-}$ as the template anion to isolate and characterize rod-like $[(EuW_{10}O_{36})_2@Ag_{72}(^t\text{BuC}{\equiv}\text{C})_{48}Cl_2]^{4+}$ (Fig. 8d).[36] The final cluster showed a higher fluorescence intensity than $[EuW_{10}O_{36}]^{9-}$ (Fig. 8e), which can be ascribed to the confinement of $[EuW_{10}O_{36}]^{9-}$ inside the Ag–alkynyl cage through Ag–O bonds, thereby reducing the energy loss caused by molecular vibrations.

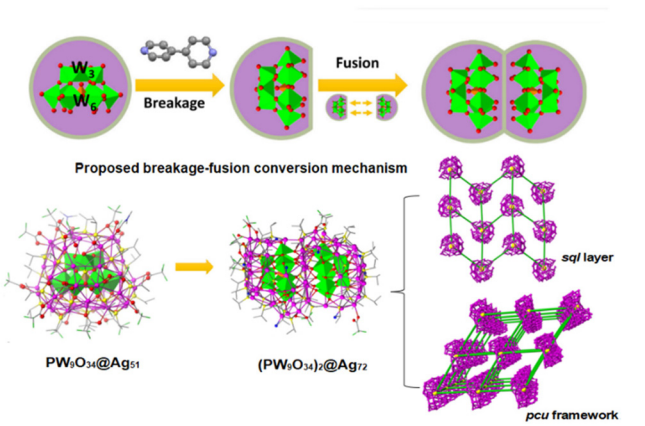

Fig. 6 Molecular structures of **$PW_9O_{34}@Ag_{51}$** and **$(PW_9O_{34})_2@Ag_{72}$** (left), and the two simplified networks with **$(PW_9O_{34})_2@Ag_{72}$** as the node (yellow balls) and bipy as the linker (right). Reproduced with permission from ref. 33. Copyright 2022, Nature Publishing Group.

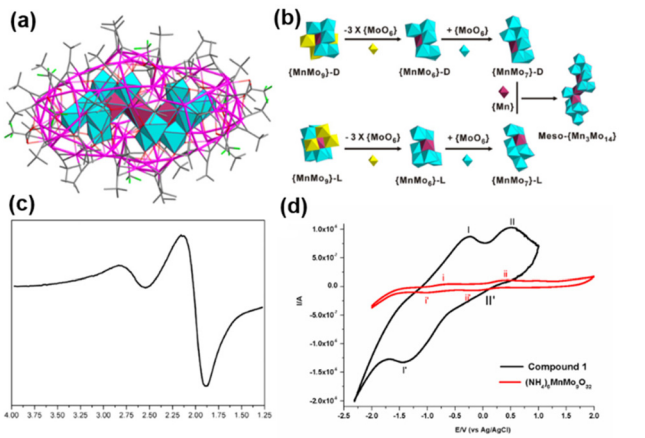

Fig. 7 (a) Single-crystal X-ray structure of **$Mn^{III}Mn^{IV}{}_2Mo_{14}O_{56}@Ag_{64}$**. (b) Illustration of *meso*-$\{Mn_3Mo_{14}\}$ from the connection of D/L-$\{MnMo_9\}$. (c) The ESR spectrum of **$Mn^{III}Mn^{IV}{}_2Mo_{14}O_{56}@Ag_{64}$**. (d) The voltammetric behaviors of $(NH_4)_6[MnMo_9O_{32}]$ (black) and **$Mn^{III}Mn^{IV}{}_2Mo_{14}O_{56}@Ag_{64}$** (red). Reproduced with permission from ref. 34. Copyright 2016, American Chemical Society.

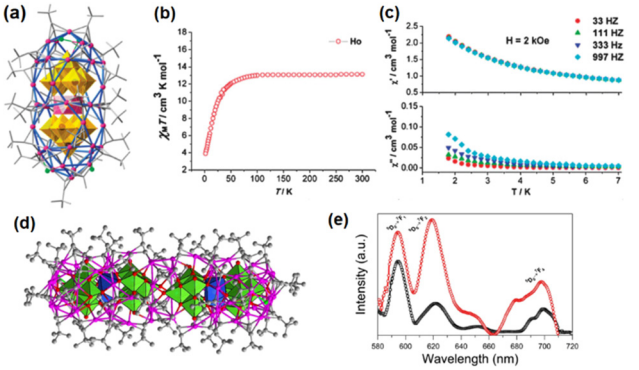

Fig. 8 (a) Molecular structure of $HoW_{10}O_{36}$@Ag_{42}. (b) Temperature dependence of the $\chi_M T$ values at 2 kOe. (c) Temperature dependence of the in-phase (χ') and out-of-phase (χ'') at different frequencies. Reproduced with permission from ref. 35. Copyright 2013, Royal Society of Chemistry. (d) Molecular structure of $(EuW_{10}O_{36})_2$@Ag_{72}. (e) The solid-state emission spectra of $(EuW_{10}O_{36})_2$@Ag_{72} (red) and $Na_9[EuW_{10}O_{36}]$ (black). Reproduced with permission from ref. 36. Copyright 2018, Wiley-VCH.

The above investigation underscores the following aspects: (1) both isopolyoxoanions and heteropolyoxoanions can effectively shape the geometries of silver clusters; (2) some flexible isopolyoxoanion precursors tend to transform into template anions with stronger coordination ability to Ag atoms in silver cluster generation, whereas most of the heteropolyoxoanions can retain their original compositions and structures; (3) employing functional MOs is an efficient strategy for introducing unique physical properties into the cluster system. For example, the enhancement in fluorescence intensity is attributed to the confinement of POMs inside the Ag shell; a core–shell electronic communication is observed in the POM-templated cluster; and single-molecule magnetic POMs can be encapsulated by the silver–alkynyl cage. Thus, the rational design of POM @ Ag clusters with the target functionality requires a careful consideration for POMs.

2.2. Ag core @ MO shell mode

As oxygen-donor ligands, MOs can play roles of structure-directing units and peripheral stabilizing layers for metal cores from undesired aggregation. Thus, the universality and versatility of MO ligands in the construction of well-defined Ag clusters highly deserve to be further explored. Based on the recent advancements in Ag core @ MO nanostructures, the reported MO ligands are categorized as mononuclear oxometallate ligands, POM ligands and metalloligands.

2.2.1. Ag core @ mononuclear oxometallates. Tetrahedral MO_4^- (CrO_4^-, MoO_4^- and WO_4^-) can bite $\{Ag_3\}$ vertex units and further regulate the overall configurations of the Ag clusters. The introduction of CrO_4^{2-} into silver–alkynyl systems gave rise to $Ag_{48}(C{\equiv}C^tBu)_{20}(CrO_4)_7$ with a pseudo-5-fold symmetric metal skeleton.[37] As illustrated in Fig. 9a, the Ag_{48} core can be viewed as a Ag_{23} cylinder encircled by an outer Ag_{25} shell. The two CrO_4^{2-} anions are located at the two poles of

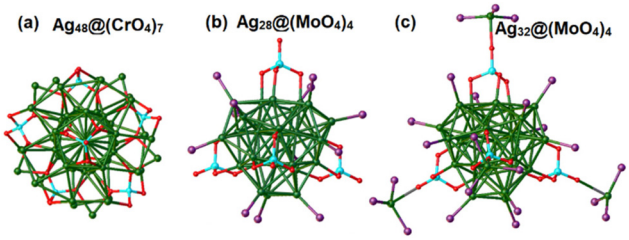

Fig. 9 View of the arrangement of MoO_4^{2-} anions on the surfaces of (a) $Ag_{48}(C{\equiv}C^tBu)_{20}(CrO_4)_7$, (b) $Ag_{28}(dppb)_6(WO_4)_4$ and (c) $[Ag_{32}(dppb)_{12}(MoO_4)_4]^{4+}$.

the Ag_{23} cylindrical kernel and the additional five CrO_4^{2-} anions are anchored onto the equator region. Lu's group reported mononuclear oxometallates and phosphine ligand co-protected superatomic silver nanoclusters including $Ag_{28}(dppb)_6(MoO_4)_4$, $Ag_{28}(dppb)_6(WO_4)_4$ and $[Ag_{32}(dppb)_{12}(MoO_4)_4]^{4+}$ (Fig. 9b and c).[38] The structure of the Ag_{28} core possesses a pyramidal geometry with four Ag_6 facets capping the four faces of the Ag_4 tetrahedron to form a two-shell Ag_4@Ag_{24} core. The tetrahedral MO_4^{2-} anions are mounted over four triangular faces of the inner Ag_4 tetrahedron of the Ag_{28} core and induce the tetrahedral geometry of the final clusters. In $[Ag_{32}(dppb)_{12}(MoO_4)_4]^{4+}$, an additional four Ag atoms are grafted on the O atoms of the MoO_4^{2-} anion, giving rise to four $MoO_4Ag(dppb)_3$ surface motifs.

2.2.2. Ag core @ POMs. Compared with mononuclear oxometallates, POMs with polyatomic backbones can enwrap and stabilize the Ag core more effectively. Notably, POMs play a protective role, and meanwhile enrich the physical and chemical properties of the Ag clusters, thus improving the catalytic performance.

Employment of POMs with selective charge distribution can be a pivotal step towards the **Ag core @ POM** configuration. As shown in Fig. 10a, Jansen and Gruber reported $[CO_3@Ag_{42}(C{\equiv}C^tBu)_{27}(CH_3CN)_2(CoW_{12}O_{40})_2]^+$ ($\mathbf{Ag_{42}@\{CoW_{12}O_{40}\}_2}$) formed by two Keggin $[CoW_{12}O_{40}]^{6-}$ units sandwiching a toroidal shaped Ag_{42} cluster. The upper and lower ends of the silver toroid are recessed, and it contains an outer cylinder of nine Ag_6 rings joined by their trans edges and a $\{Ag_6CO_3\}$ unit located at the midpoint height of the Ag_{36} cylinder.[39] Ozeki's group reported $[CO_3@Ag_{42}(C{\equiv}C^tBu)_{27}(SiW_9Nb_3O_{40})_2]^-$ ($\mathbf{Ag_{42}@\{SiW_9Nb_3O_{40}\}_2}$), in which two Nb-substituted Keggin

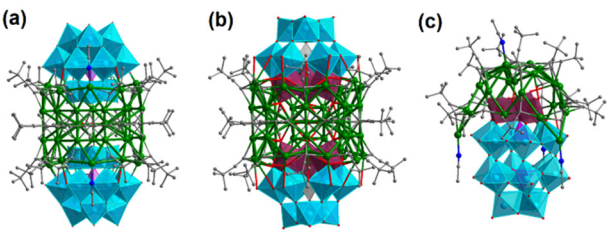

Fig. 10 Molecular structures of (a) $\mathbf{Ag_{42}@\{CoW_{12}O_{40}\}_2}$, (b) $\mathbf{Ag_{42}@\{SiW_9Nb_3O_{40}\}_2}$ and (c) $\mathbf{Ag_{25}@P_2W_{15}Nb_3O_{62}}$.

$[\alpha\text{-A-}SiW_9Nb_3O_{40}]^{7-}$ polyoxotungstates cap both the openings of a toroidal Ag_{42} cluster (Fig. 10b),[40] identical to the silver toroid of $\mathbf{Ag_{42}@\{CoW_{12}O_{40}\}_2}$. The largest structural dissimilarity between the two clusters lies in the binding sites of the Keggin polyoxometalates to the toroidal Ag_{42} clusters. The Ag_{42} cluster in $\mathbf{Ag_{42}@\{SiW_9Nb_3O_{40}\}_2}$ shows affinity to the corner-shared triad of $[WO_6]$ octahedra, while $\mathbf{Ag_{42}@\{CoW_{12}O_{40}\}_2}$ favors assembling with the corner-shared triad. They amplified the selective doping of less positively charged Nb(v) which increased the surface negative charge of the corner-shared triad, leading to an opposite preference for the binding site compared to the unsubstituted analogue. This result indicates that the binding site of metal-oxo clusters can be modulated by tuning the surface electron density. In the two hybrid compounds, silver alkynyl and polyoxometalate moieties are symmetrically connected. The addition of $[^nBu_4N]_5H_4[P_2W_{15}Nb_3O_{62}]$ to a CH_3CN solution containing ^{t}BuC≡CAg and AgOTf led to the formation of an asymmetrically fused polyoxometalate–silver alkynide composite cluster, $[Ag_{25}(C{\equiv}C^tBu)_{16}(CH_3CN)_4(P_2W_{15}Nb_3O_{62})]$ ($\mathbf{Ag_{25}@P_2W_{15}Nb_3O_{62}}$), where 25 Ag atoms are selectively attached to the Nb-substituted hemisphere of the pedestal Dawson $[\alpha\text{-}P_2W_{15}Nb_3O_{62}]^{9-}$ (Fig. 10c).[41] Cronin and coworkers isolated $[Ag_{18}Cl@(Te_3W_{38}O_{134})_2]$ with C_2 symmetry, whose $Ag_{18}Cl$ fragment is supported by two superlacunary $[Te_3W_{38}O_{134}]^{28-}$ frameworks.[42]

The lacunary POM clusters have more well-defined vacant sites and higher negative charges compared to the plenary POMs. Hence, lacunary POMs are expected to assemble with electrophilic Ag clusters to generate the "Ag cluster within POM cluster" skeleton. By employing lacunary silicotungstate ligands, a series of Ag clusters encapsulated by two or more silicotungstate ligands have been designed with unique structures. Mizuno and coworkers obtained $[Ag_4@(\gamma\text{-}H_2SiW_{10}O_{36})_2(DMSO)_2]^{8-}$ ($\mathbf{Ag_4@\{SiW_{10}O_{36}\}_2}$), with diamond-shaped $[Ag_4]^{4+}$ stabilized in the lacunary pocket of $\{SiW_{10}\}$ (Fig. 11a).[43] Compared to the AgOAc or POMs, $\mathbf{Ag_4@\{SiW_{10}O_{36}\}_2}$ showed better catalytic performance in the hydrolytic oxidation of silanes to silanols. With the same Ag salt and silicotungstate ligands, they synthesized $[Ag_6(\gamma\text{-}H_2SiW_{10}O_{36})_2]^{8-}$ ($\mathbf{Ag_6@\{SiW_{10}O_{36}\}_2}$) using Ph_2SiH_2 as the reducing agent.[44] The structural analysis indicates that the octahedron-shaped $[Ag_6]^{4+}$ core is sandwiched by two lacunary $\{SiW_{10}\}$ units (Fig. 11b). Unfortunately, $\mathbf{Ag_6@\{SiW_{10}O_{36}\}_2}$ was quickly decomposed in organic solvents such as acetone, CH_3CN, and DMF. With such an assembly strategy, they continued to report a novel fcc-type $[Ag_7]^{5+}$ core stuffed inside an unprecedented triangular hollow $[Si_3W_{27}O_{96}]^{18-}$ framework (Fig. 11c).[45] Hence, $\mathbf{Ag_7@Si_3W_{27}O_{96}}$ exhibited much higher stability than $\mathbf{Ag_6@\{SiW_{10}O_{36}\}_2}$. Recently, Suzuki's group achieved the assembly of trefoil-propeller-shaped $\{Ag_{27}\}^{17+}$ surrounded by three open-Dawson-type $[Si_2W_{18}O_{66}]^{16-}$ units (Fig. 11d),[46] and they explored the assembly processes of $\mathbf{Ag_{27}@\{Si_2W_{18}O_{36}\}_3}$ on the basis of mass spectrometry analysis: initially, $\{Si_2W_{18}\}$ protected Ag_2 possessing large vacant sites can accommodate an additional four Ag atoms to give an octahedral Ag_6 cluster. Subsequently, hcp-type Ag_9 can assemble

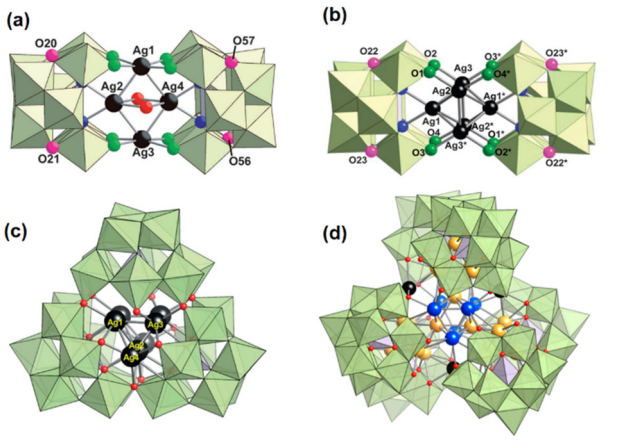

Fig. 11 (a) Polyhedral and ball-and-stick representation of $\mathbf{Ag_4@(SiW_{10}O_{36})_2}$. Reproduced with permission from ref. 43. Copyright 2012, Wiley-VCH. (b) Polyhedral and ball-and-stick representation of $\mathbf{Ag_6@(SiW_{10}O_{36})_2}$. Reproduced with permission from ref. 44. Copyright 2013, Royal Society of Chemistry. (c) Polyhedral and ball-and-stick representation of $\mathbf{Ag_7@Si_3W_{27}O_{96}}$. Reproduced with permission from ref. 45. Copyright 2020, Wiley-VCH. (d) Polyhedral and ball-and-stick representation of $\mathbf{Ag_{27}@(Si_2W_{18}O_{36})_3}$. Reproduced with permission from ref. 46. Copyright 2019, American Chemical Society.

with such three $\{Si_2W_{18}\text{-}Ag_6\}$ and then aggregate into $\mathbf{Ag_{27}@\{Si_2W_{18}O_{66}\}_3}$. These results will enhance our current understanding of the formation mechanism of metal-oxo-cluster-protected silver clusters. Further research reveals that $\mathbf{Ag_{27}@\{Si_2W_{18}O_{66}\}_3}$ exhibits ultrastability in organic solvents and a unique interface between the Ag core and POM shell for efficient H_2 cleavage.[47] The $\{Si_2W_{18}\}$ module can provide storage for the generated protons on the negatively charged basic surface, whilst the mixed-valence $\{Ag_{27}\}$ core can accommodate additional electrons. Recently, they continued to report stimuli-responsive and reversible control of the electronic states of $\mathbf{Ag_{27}}$ *via* addition of an acid or base. Because the protonation/deprotonation of $[Si_2W_{18}O_{66}]^{16-}$ can cause changes in the electron donation from the POM ligands to the Ag nanocluster, consequently the electron density distribution changed.[48] These two works provide a new perspective on the unique redox and acid/base properties of the molecular hybrids of Ag nanoclusters and POMs.

In conclusion, in this section, the charge distribution of POMs is uneven on the surface, and the positive Ag cluster cores prefer to bind the partial surface of metal-oxo modules with higher negative charges, thus providing effective protection for the periphery of the silver clusters. However, it still remains a challenge to control the charge distribution of POMs. Therefore, the organic-molecule modification of MOs can be another efficient synthetic strategy to construct Ag core @ MO nanostructures.

2.2.3. Metalloligands. To ensure that oxometallates remain outside the Ag cores, we can construct metalloligands from the interaction of MOs and organic ligands to prevent the oxygen at one side of oxometallates from coordinating with silver atoms. Thus, metalloligands with pre-organized coordination

sites can only be used as a protective group on the periphery of Ag clusters.

Mo-based metalloligands. The –OH groups of thiacalixarene can ligate Mo^{VI} with the assistance of the –S– bridge to form a metalloligand with more terminal O atoms for further binding to Ag sites. Mo-based metalation on thiacalixarenes can construct metalloligands with coordination sites and continuous carbon backbones, which can provide an additional stabilization effect for Ag clusters. Recently, Sun *et al.* used $Mo^{VI}O_3^-$ anchored *p*-tertbutylthiacalix[4]arene (H4TC4A) as a metalloligand to obtain $[Cl@Ag_{42}(MoO_3\text{–}TC4A)_6(RS)_{18}]^-$ (**Ag_{42}**) nanoclusters (Fig. 12a).[49] With such a stepwise assembly strategy, they continued to synthesize hexagonal $Ag_{18}(Mo_2O_5PTC4A)_6(EtS)_6(Tos)_2$ (**Ag_{18}-a**) and rectangular $Ag_{18}S\{Mo_2O_5(PTC4A)_2(MoO_2{}^nPrO)[MoO(^nPrO)_2]\}_2(CyS)_6(Tos)_2(^nPrO)_2$ (**Ag_{18}-b**) from the reaction of H4PTC4A, $(^nBu_4N)_4(\alpha\text{-}Mo_8O_{26})$ and $[RSAg]_n$. As shown in Fig. 12b, a $[Mo^{VI}{}_2O_5PTC4A]^{12-}$ metallamacrocycle is constructed from the ligation of $PTC4A^{4-}$ to two $\{MoO_3\}$ units by using sulfur atoms and phenol oxygen atoms.[50] The condensation process of the metalloligand is blocked by propan-1-ol ligation, thereby causing the structural dissimilarity between **Ag_{18}-a** and **Ag_{18}-b**. More notably, **Ag_{18}-a** showed high charge separation efficiency and photothermal conversion ability.

Ti-based metalloligands. One of the most interesting aspects of Ti-based metalloligands lies with the fact that these titanium-oxo modules can be viewed as transferable building blocks or synthons of TiO_2. As shown in Fig. 13a, titanium-based metalloligands with trifurcate TiL_3 moieties (L = salicylate) serve as a cornerstone for the generation of a series of Ag–S clusters possessing a pyramidal geometry, capping the vertices of the $\{Ag_3\}$ triangular subunits.[51] Zang's group employed such a synthetic strategy to encapsulate all-carboxylate-protected 2e Ag clusters into two novel Ti-based coordination

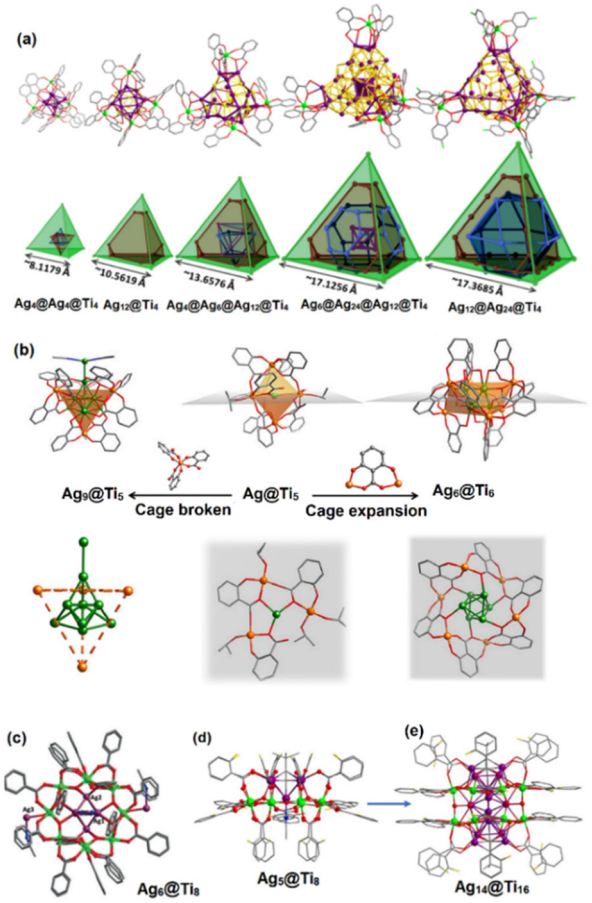

Fig. 13 (a) Molecular structures (top) and illustrations (bottom) of a series of $Ag_n@Ti_4$. Reproduced with permission from ref. 51. Copyright 2020, American Chemical Society. (b) A single Ag(I) atom or Ag cluster confined in Ti cages. Reproduced with permission from ref. 52. Copyright 2020, Springer. Molecular structures of (c) **$Ag_6@Ti_8$**, (d) **$Ag_5@Ti_8$** and (e) **$Ag_{14}@Ti_{16}$**. Reproduced with permission from ref. 53 and 54. Copyright 2018 and 2021, Wiley-VCH.

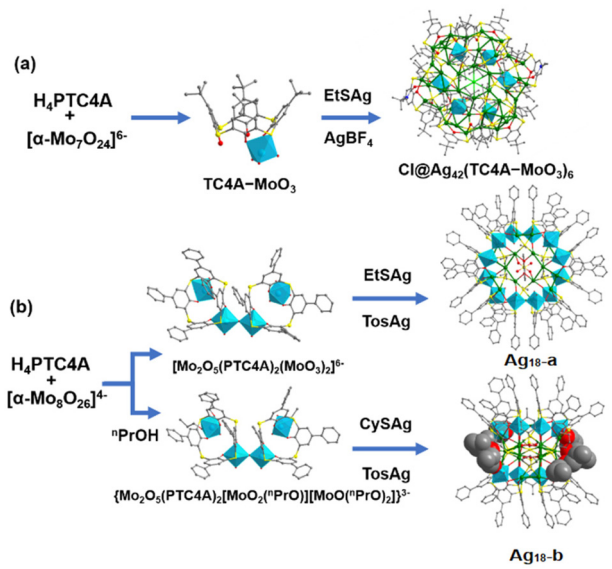

Fig. 12 Stepwise synthetic routes for (a) **Ag_{42}** and (b) **Ag_{18}-a** and **Ag_{18}-b**.

cages based on salicylic acid and its derivatives, which exhibit optical limiting effects in DMF solution and temperature-dependent photoluminescence properties.[52] The molecular structures of $(TBA)_2\{Ag_6Ti_6(Sal)_x(L_1)_6(HL_1)_{6-x}\}$ (**$Ag_6@Ti_6$**) and $(Ag(CH_3CN)_3)\{Ag_9Ti_4(Sal)_{12}(CH_3CN)_3\}$ (**$Ag_9@Ti_5$**) are presented in Fig. 13b. In addition to the TiL_3 moieties, the hollow-like Ti-oxo ring stabilized by benzoate ligands can provide sufficient oxygen sites inside the cavity for the coordination of silver ions. Zhang *et al.* constructed triple core–shell $Ag_6@Ti_{16}@(benzoate)_{26}$ nanoclusters (**$Ag_6@Ti_{16}$**) by wrapping the subvalent Ag_6 octahedron with two macrocyclic Ti_8O_{40} clusters through Ag–O–Ti coordination interactions (Fig. 13c).[53] The Ag_6 cluster inserted inside the cricoid Ti_{16}-oxo shell adopts different geometric configurations, which contribute to different optical limiting activities. However, **$Ag_6@Ti_{16}$** still suffers from poor stability and is easily dissociated in moisture due to the inner Ag core terminated with weak CH_3CN solvents. Subsequently, the **$Ag_5@Ti_8$** core–shell nanocluster, whose Ag_5 is terminated with ^{t}BuC≡C– and CH_3CN, was

obtained through the introduction of alkyne ligands and silver ions into the synthetic reaction system of Ti_8O_{40}. To preclude the frailty of CH_3CN, the reaction conditions were further modulated through a replacement of acetonitrile with toluene. Consequently, the Ag_{14} nanorod @ Ti_{16}-oxo nanoring was successfully obtained, whose Ag_{14} core can be viewed as two pyramidal Ag_5 sandwiching a rhombus Ag_4 unit through argentophilic interactions (Fig. 13d and e).[54] **Ag_{14}@Ti_{16}** represents the first example of Ag clusters synergistically stabilized by alkynyl and Ti-oxo cluster shells. The robust protecting shell of **Ag_{14}@Ti_{16}** accounts for its superhydrophobicity and excellent ambient stability. In summary, anchoring an organic ligand on the partial surface of Ti-oxo clusters can be an effective approach to avoid coordination to additional Ag atoms.

Yb-based metalloligands. Lanthanide-oxo clusters have attracted considerable attention in view of their magnetic, catalytic, and luminescence properties. Nevertheless, little effort has been focused on the combination of Ag clusters and Ln-oxo clusters. In 2018, Xie and his coworkers presented the first Ag–Yb clusters (Fig. 14a), namely, $[Cl@Ag_{16}(C{\equiv}C^tBu)_9(hfac)(CH_3CO_2)]$-$[Yb_3(\mu_3\text{-}OH)_3(^tBuPO_3)_3(hfac)_3(CH_3OH)_3]$ (**Ag_{16}-Yb_3**) and $[Cl@Ag_{16}(C{\equiv}C^tBu)_7(hfac)_2(^tBuPO_3)]_2$-$[Yb_6(\mu_3\text{-}OH)_2(\mu_3\text{-}O)_6(^tBuPO_3)_6(CH_3OH)_6(H_2O)_6]$ (**{Ag_{16}}$_2$-Yb_6**).[32] In **Ag_{16}-Yb_3**, each Yb(III) atom of the cap-shaped trinuclear $[Yb_3(\mu_3\text{-}OH)(\mu_3OH)_3]^{6+}$ subunit is coordinated by one hexafluoroacetylacetone (hfac), and each $^tBuPO_3^{2-}$ binds two Yb and five Ag atoms, thereby leading to the connection of a silver alkynyl cluster with a hydroxoytterbium phosphonate cluster. As shown in Fig. 14b, the octahedral $[Yb_6(\mu_3\text{-}OH)_2(\mu_3\text{-}O)_6]^{4+}$ subunit is sandwiched by two silver alkynyl clusters, which can be viewed as a fusion of two **Ag_{16}-Yb_3**.

Based on all of the above points, the construction of such stable Ag core @ MO clusters requires robust MO shells to preclude hydrolysis reactions in moisture and abundant oxo sites to anchor Ag atoms efficiently. Additionally, incorporation of some organic ligands (alkynyls, *etc.*) and MO shells can prevent the exposure of Ag clusters to the humid environment, thus providing collaborative stabilization of Ag cores.

2.3. Ag core @ MO @ Ag shell mode

We have witnessed the fruitful advancements in POM-templated Ag(I) clusters, but multi-shell POM-templated superatomic Ag clusters are rarely observed in the literature. This is because achieving the fast kinetics of the reduction process by $NaBH_4$ is a major challenge to control the complicated assembly process of $Ag^{+1/0}$ species and metal-oxo modules in multi-shell nanostructures. Tremendous efforts have been made in developing effective and efficient synthetic methods to slow down the reduction process and obtain molecularly pure POM-templated superatomic Ag clusters.

Recently, Sun and coworkers adopted a strategy combining an anion template and solvent–intervention in the assembly of silver nanoclusters and then harvested a series of stable crystalline products. In 2018, they used a binary solvent system (CH_3OH/DMF) to obtain $Ag_6@(MoO_4)_7@Ag_{56}(MoO_4)_2(^iPrS)_{28}(p\text{-}TOS)_{14}(DMF)_4$ (**Ag_6@(MoO_4)$_7$@Ag_{56}**) possessing a seven-fold symmetric wheel-like topology.[24] As shown in Fig. 15a, the cluster-in-cluster structure comprises an octahedral Ag_6^{4+} kernel trapped in the centre of the Ag_{56} nanowheel with seven MoO_4^{2-} anion templates around it. Two additional MoO_4^{2-} anions serve as hubcaps of the wheel. MoO_4^{2-} anions play binary roles of a template to support the outermost Ag shell and inorganic ligands. Subsequently, they adopted the same synthetic method to prepare a hierarchical multi-shell structure $Ag_{10}@(MoO_4)_7Ag_{60}(^tBuC_6H_4S)_{33}(mbc)_{18}(DMF)(H_2O)_2$ (**Ag_{10}@(MoO_4)$_7$@Ag_{60}**), whose Ag_{60} shell was further protected by *m*-methoxybenzoic acid (mbc), $^tBuC_6H_4S$ and solvent molecules.[16] Seven MoO_4^{2-} anions are arranged in the interstice between the Ag_{10} core and the Ag_{60} shell. They continued to synthesize a three-layered core–shell $Ag_{10}@(Mo_7O_{26})_2@Ag_{70}(MoO_4)_2(CyhS)_{36}(CF_3SO_3)_{16}(DMF)_6$ (**Ag_{10}@(Mo_7O_{26})$_2$@Ag_{70}**) with the outermost shell capped by $CyhS^-$, $CF_3SO_3^-$, MoO_4^{2-} and solvent molecules.[55] This work establishes a one-pot synthesis of mixed-valence $Ag^{0/1+}$ clusters with *in situ*-generated POMs in the interlayer. The Ag_{10} inner core (**Ag_{10}-1**) of **Ag_{10}@**

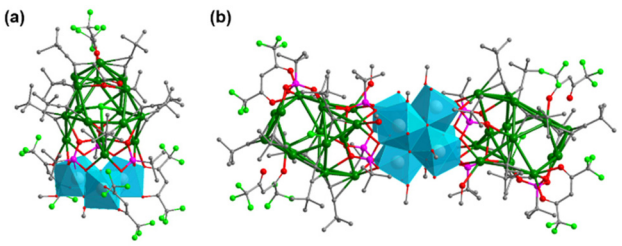

Fig. 14 Molecular structures of (a) **Ag_{16}-Yb_3** and (b) **{Ag_{16}}$_2$-Yb_6**.

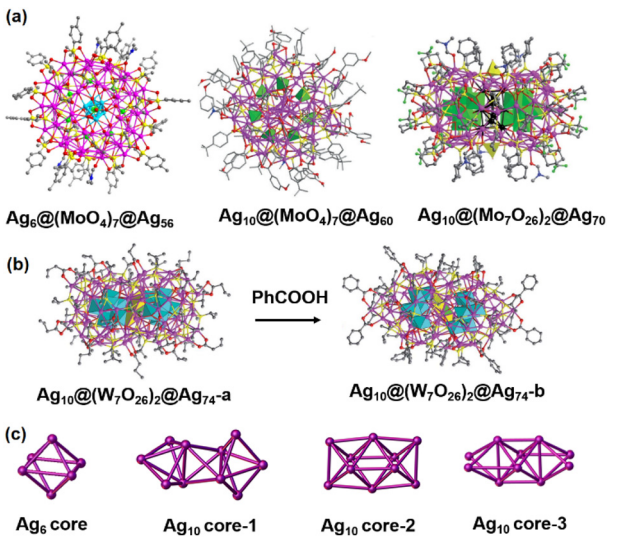

Fig. 15 (a) A summary of Ag clusters adopting the Ag core @ MO @ Ag shell mode. (b) Structural conversion of **Ag_{10}@(W_7O_{26})$_2$@Ag_{74}-a** and **Ag_{10}@(W_7O_{26})$_2$@Ag_{74}-b**. (c) The inner Ag cores of these Ag clusters. Reproduced with permission from ref. 24. Copyright 2018, Nature Publishing Group. Reproduced with permission from ref. 16. Copyright 2019, Wiley-VCH. Reproduced with permission from ref. 55 and 56. Copyright 2019, Royal Society of Chemistry.

$(MoO_4)_7$@Ag_{60} is constructed from two bipyramids sharing one edge with the central tetrahedron, whilst the fcc-structured Ag_{10} core (**Ag_{10}-2**) captured in **Ag_{10}@$(Mo_7O_{26})_2$@Ag_{70}** can be seen as a fusion of two single-edge opened Ag_6 octahedra sharing an edge. In addition to the Mo-based POMs, they used WO_4^{2-} as the MO percursor to obtain Ag_{10}@$(W_7O_{26})_2$@$Ag_{74}S_2$(^{i}PrS)$_{40}$(^{n}PrCOO)$_{18}$ (**Ag_{10}@$(W_7O_{26})_2$@Ag_{74}-a**) and Ag_{10}@$(W_7O_{26})_2$@$Ag_{74}S_2$(^{i}PrS)$_{40}$(PhCOO)$_{18}$ (**Ag_{10}@$(W_7O_{26})_2$@Ag_{74}-b**) displaying silver shell isomerism.[56] The two clusters share the same innermost Ag_{10} core (**Ag_{10}-3**), which can be considered as an Ag_6 octahedron capped by four additional silver tetrahedra. **Ag_{10}-3** is symmetrically wrapped by two crescent-shaped $[W_7O_{26}]^{10-}$units, and the Ag_{10}@$(W_7O_{26})_2$ fragment is enclosed in a silver shell shaped as flat-headed (**Ag_{10}@$(W_7O_{26})_2$@Ag_{74}-a**) and cuspidal prolate spheres (**Ag_{10}@$(W_7O_{26})_2$@Ag_{74}-b**), respectively. Interestingly, PhCOOH can induce a one-way transformation from **Ag_{10}@$(W_7O_{26})_2$@Ag_{74}-a** to **Ag_{10}@$(W_7O_{26})_2$@Ag_{74}-b** (Fig. 15b), which represents the first example of carboxylate-stimulated shell isomerism in silver nanoclusters. In the preparation of the five multi-shell nanoclusters mentioned above, the aldehyde group of DMF can not only offer O donors with coordination affinity for Ag atoms, but also function as a mild reductant, thus leading to a kinetics-controlled growth course during assembly. Based on all the above, this solvent-intervention approach yielded a series of complicated multi-shell nanostructures containing reductive silver cores, thus providing a deeper insight into silver nanocluster assembly, flexibility and reactivity.

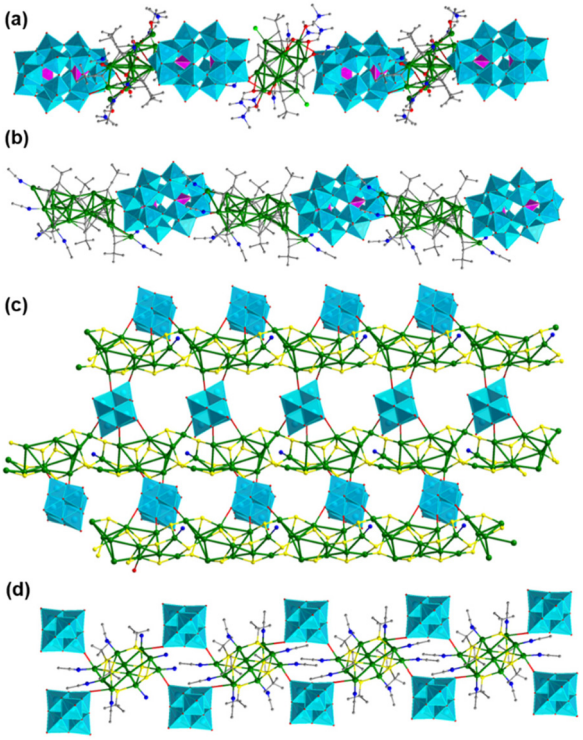

Fig. 16 Packing diagram of (a) $\{[Ag_{14}(C{\equiv}C^tBu)_8(C_3H_7NO)_{10}][Ag_{12}(C{\equiv}C^tBu)_6Cl(DMF)_{10}]H[P_2W_{18}O_{62}]_2\}_n$, (b) $\{[Ag_{16}(C{\equiv}C^tBu)_{11}(CH_3CN)_6][P_2W_{18}O_{62}]\}_n$, (c) $\{[Ag_{11}(^i BuS)_9(CH_3CN)](Mo_6O_{19})\}_n$ and (d) $[Ag_{10}(S^tBu)_6(CH_3CN)_8(Mo_6O_{19})_2]_n$.

2.4. Coordination polymers

Based on all of the above results, various core–shell MO–Ag composite clusters have been successfully constructed. Besides this, MOs and Ag clusters can be facile candidates for generating coordination polymers through Ag–O bonds. The effort to realize the co-assembly of POMs and Ag clusters into coordination polymers aims to discover new properties due to cooperative effects.[57,58] Unambiguous determination of the structures of such polymers is critically important to understand inherent assembly rules, although it is a big challenge due to the difficulties in obtaining X-ray quality single crystals. As shown in Fig. 16a and b, Jansen and Gruber prepared the first chain-like polymeric compounds $\{[Ag_{14}(C{\equiv}C^tBu)_8(C_3H_7NO)_{10}][Ag_{12}(C{\equiv}C^tBu)_6Cl(DMF)_{10}]H[P_2W_{18}O_{62}]_2\}_n$ and $\{[Ag_{16}(C{\equiv}C^tBu)_{11}(CH_3CN)_6][P_2W_{18}O_{62}]\}_n$ in 2011, which are constructed from the linkage of the Wells–Dawson $[P_2W_{18}O_{62}]^-$ and the silver alkynyl cluster building blocks through direct Ag–O–W bridges.[59] These results indicated that the O-donor inorganic ligands can indeed act as bridging ligands in the formation of higher dimensional Ag cluster-based frameworks. By using Lindqvist-type $[Mo_6O_{19}]^{2-}$ in place of $[P_2W_{18}O_{62}]^{6-}$, a two-dimensional infinite sheet $\{[Ag_{11}(^i BuS)_9(CH_3CN)](Mo_6O_{19})\}_n$ was constructed by connecting thiolate-bridged Ag_{11}-based chain-like motifs and $[Mo_6O_{19}]^{2-}$ anions through Ag–O coordination interaction (Fig. 16c).[60] Zang' group introduced $[Mo_6O_{19}]^{2-}$ into Ag–S systems to synthesize another coordination polymer $[Ag_{10}(S^tBu)_6(CH_3CN)_8(Mo_6O_{19})_2]_n$ (Fig. 16d),[61] which exhibits green photoluminescence at room temperature. In these silver–MO aggregations, MOs played a special role similar to an organic linker in extending the discrete Ag clusters to the higher dimensionality.

2.5. Interclusters

When the coordination sites on the Ag cluster surface are occupied by organic ligands, the formation of Ag–O bonds meets with obstruction, resulting in inaccessibility to POM–Ag-based MOFs. Herein, Ag clusters with positive charges can co-assemble with negatively charged POMs through electrostatic attraction to form well-defined intercluster compounds. Well-ordered crystalline arrangements would demand a selection of suitable building blocks with long-range Coulomb interactions and a size matching relationship. Jansen and coworkers obtained a series of $[Ag_{14}(C{\equiv}C^tBu)_{12}]$-POMs (POM = $[W_6O_{19}]^{2-}$, $[PW_{12}O_{40}]^{3-}$, and $[SiMo_{12}O_{40}]^{4-}$), in which O_h-symmetry $\{Ag_{14}(C{\equiv}C^tBu)_{12}\}$ fragments are stacked with POM anions into electrostatic force-induced assemblies. POMs can contribute much more than counterions in charge balance. Employing functional POMs is expected to endow the intercluster compounds with special properties. Wang's group chose $[Ag_{62}S_{13}(S^tBu)_{32}]^{4+}$ and $[Mo_6O_{19}]^{2-}$ as building units for **Ag_{62}-$(Mo_6O_{19})_2$** (Fig. 17a).[62] As depicted in Fig. 17b, the charge-transfer behavior was firstly observed and presented as an emission switching property. Besides Ag(I) cluster-based assemblies, Zhu's group isolated Ag nanocluster-based assem-

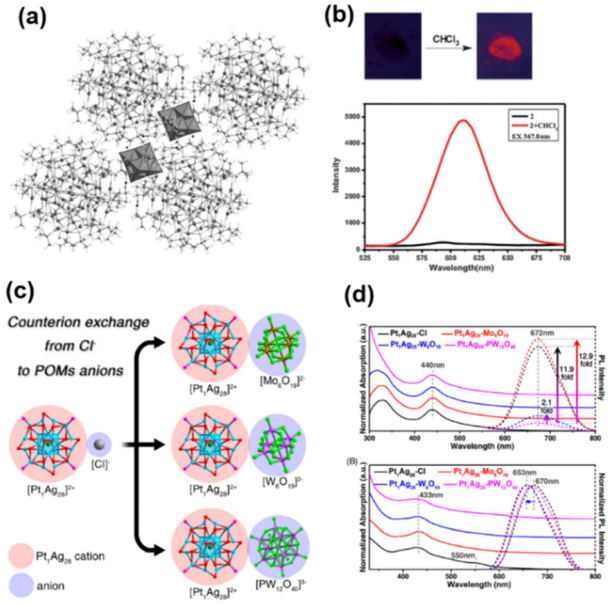

Fig. 17 (a) Packing diagram and (b) luminescence change induced by $CHCl_3$ of $[Ag_{62}S_{13}(S^tBu)_{32}][Mo_6O_{19}]_2$. Reproduced with permission from ref. 62. Copyright 2012, Wiley-VCH. (c) Structures and the optical absorptions and (d) emissions of Pt_1Ag_{28}–Mo_6O_{19}, Pt_1Ag_{28}–W_6O_{19} and Pt_1Ag_{28}–$PW_{12}O_{40}$. Reproduced with permission from ref. 63. Copyright 2021, American Chemical Society.

blies exhibiting crystalline-state optical properties through manipulation of $[Pt_1Ag_{28}(SAdm)_{18}(PPh_3)_4]^{2+}$ and POM counterions (Fig. 17c and d).[63] It is worth noting that the same $[Mo_6O_{19}]^{2-}$ precursors can connect $Ag_{10}(S^tBu)_6(CH_3CN)_8$ [61] through Ag–O bonds to form coordination polymers in section 2.4. It is virtually impossible for $\{Pt_1Ag_{28}(SAdm)_{18}(PPh_3)_4\}$ to accommodate $[Mo_6O_{19}]^{2-}$ due to the steric hindrance of the bulky thiolate ligands.

2.6. Mixed array configurations

Virtually, MOs can play dual roles of a peripheral ligand and templating agent in the synthesis of Ag clusters. As depicted in Fig. 18a, Mak *et al.* obtained $[(O_2)V_2O_6]_3@Ag_{43}(C{\equiv}CPh)_{19}@[(^tBuPO_3)_4V_4O_8]_3$ (**$[[(O_2)V_2O_6]_3@Ag_{43}@[(^tBuPO_3)_4V_4O_8]_3]$**) through the reaction of polyoxovanadates with AgC≡CPh, $AgNO_3$, and $^tBuPO_3H_2$ in the presence of H_2O_2. It is noteworthy that the surface $[(^tBuPO_3)_4(V_4O_8)]^{4-}$ moiety is connected to the peroxo group in $[(O_2)V_2O_6]^{4-}$ to construct $[(^tBuPO_3)_4(V_4O_8)(O_2)(V_2O_6)]^{8-}$, which penetrates the Ag_{43} skeleton.[64] Later, they continued to report $(^tBuPO_3)_4V_4O_8$-capped $\{[(O_2)V_2O_6]_2@Ag_{36}(C{\equiv}C^tBu)_{12}[(^tBuPO_3)_4V_4O_8]_2(^tBuPO_3)_2(NO_3)_7(Py)(DMF)\}^{3+}$ (**$[[(O_2)V_2O_6]_2@Ag_{36}@[(^tBuPO_3)_4V_4O_8]_2]$**),[65] encapsulating a pair of $[(O_2)V_2O_6]^{4-}$ (Fig. 18b). Shortly, they harvested $[(V_2O_7)_2@Ag_{44}(C{\equiv}C^tBu)_{14}@(V_{32}O_{96})]$ (**$(V_2O_7)_2@Ag_{44}@(V_{32}O_{96})$**),[66] in which a pyrovanadate-templated globular Ag alkynyl cluster is circumscribed by macrocyclic polyoxovanadate $[V_{32}O_{96}]^{32-}$ (Fig. 18c). As shown in Fig. 18d, MoO_4^{2-} anions simultaneously act as central templates and exterior ligands in

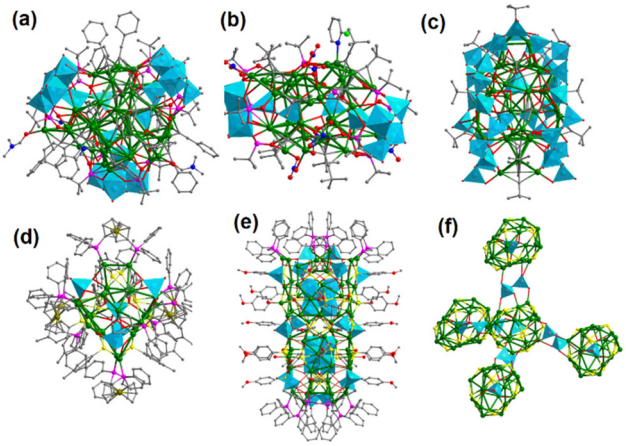

Fig. 18 Molecular structures of (a) $[(O_2)V_2O_6]_3@Ag_{43}@[(^tBuPO_3)_4V_4O_8]_3$, (b) $[(O_2)V_2O_6]_2@Ag_{36}[(^tBuPO_3)_4V_4O_8]_2$, (c) $(V_2O_7)_2@Ag_{44}@(V_{32}O_{96})$, (d) $MoO_4@Ag_{24}@(MoO_4)_4$ and (e) $(Mo_6O_{22})_2@Ag_{76}@(MoO_4)_{16}$. (f) Each $CrO_4@Ag_{20}$ subunit connected to its adjacent four neighbours by $Cr_2O_7^{2-}$. (g) Molecular structure (left) and cyclic voltammogram (right) of $SiW_{10}O_{37}@Ag_{41}$-β-$SiW_{12}O_{40}$.

$[MoO_4@Ag_{24}(MeC_6H_4S)_{12}(dppf)_6(MoO_4)_4]^{2+}$ (**$MoO_4@Ag_{24}@(MoO_4)_4$**).[21] Ulteriorly, MO_4^{2-} can aggregate into polyoxoanion templates to stabilize a silver cage. Sun's group obtained a rod-like $(Mo_6O_{22})_2@Ag_{76}(MeOC_6H_4S)_{28}(dppm)_8(MoO_4)_{16}$ (**$(Mo_6O_{22})_2@Ag_{76}@(MoO_4)_{16}$**) cluster with an S_4-symmetry kernel.[17] The 76-nucleus nanocluster is templated by two bicubane $Mo_6O_{22}^{8-}$ anions *in situ* generated from MoO_4^{2-} anions, and the outer silver shell is protected by other MoO_4^{2-} anions (Fig. 18e). **$(MoO_4)_5@Ag_{52}S_6@(MoO_4)_{10}$**[17] mentioned in section 2.1.1 and **$Ag_6@(MoO_4)_7@Ag_{56}@(MoO_4)_2$**[24] in section 2.3 also display such structural types. Dual roles of MOs can also be observed in high-dimensional frameworks. Sun and his partners isolated enantiomeric chiral 3D frameworks of $[CrO_4@Ag_{20}(^iSPr)_{10}(Cr_2O_7)_2(COOCF_3)_4(DMF)_4]_n$ through spontaneous resolution, encapsulating one CrO_4^- as a template, and two $Cr_2O_7^{2-}$ anions serve as bridges to connect the neighboring **$CrO_4@Ag_{20}$** node (Fig. 18f).[14]

In addition to the dual roles of ligands and templates, POMs can function simultaneously as templates and counterions for Ag clusters. Wang's group obtained $[\alpha\text{-}SiW_{10}O_{37}@Ag_{41}(^tBuC{\equiv}C)_{27}(CH_3CN)_3][\beta\text{-}SiW_{12}O_{40}]$ by encapsulation of the

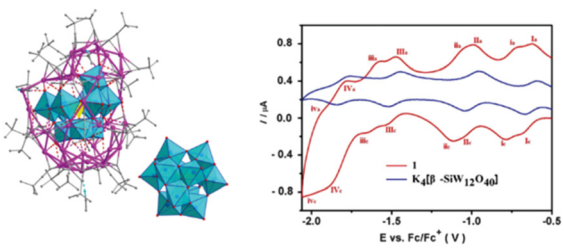

Fig. 19 Molecular structure (left) and cyclic voltammogram (right) of $SiW_{10}O_{37}@Ag_{41}$-β-$SiW_{12}O_{40}$. Reproduced with permission from ref. 67. Copyright 2016, Royal Society of Chemistry.

dilacunary silicodecatungstate.[67] In the generation of Ag clusters, the precursor $[\gamma\text{-}SiW_{10}(H_2O)_2O_{34}]^{4-}$ is transformed to $[\alpha\text{-}SiW_{10}O_{37}]^{10-}$ and $[\beta\text{-}SiW_{12}O_{40}]^{4-}$, which play respective roles of templating agents and counterions. As illustrated in Fig. 19, interesting electrochemical behaviours can be observed with the stable Ag_{41} cage as an electron transfer mediator and the two silicotungstate clusters as multiple electro-redox centers.

3. Conclusions

Overall, the formation of atomically precise MO–Ag cluster nanocomposites can facilitate the establishment of structure-effect relationships of Ag nanoparticle-transition metal oxide materials at atomic scale. The minireview is concluded by briefly outlining the roles of MOs in the formation of a variety of silver clusters. MOs act as not only templates encapsulated by silver shells but also multidentate inorganic ligands at the periphery of the silver core. Besides, MOs can be embedded into the interspace between the Ag core and Ag shell. In addition to Ag–O coordinative assemblies, the cationic Ag clusters and anionic POMs are basic units for the assembly of intercluster compounds *via* electrostatic forces. The sizes, charge distribution, and structural topologies of the MO/Ag clusters can influence array configurations. Moreover, ligands, solvents and the pH of the assembly environment can cause structural modulation of the final cluster composites. Furthermore, functional MOs can be an important parameter to control the physicochemical properties including electron communication, luminescence thermochromism, single-molecule magnetism, stability and optical limiting effects of the final composite clusters. Thus, research studies on MO–Ag clusters have been relatively systematic and comprehensive in terms of synthesis and properties.

Nevertheless, the specific contribution and action mechanism of MOs towards the properties of cluster composites still remain unclear to date. The deeper understanding needs further systematic research in the future. Meanwhile, despite the similarities in the physical and chemical properties of coinage metal nanoclusters (Cu, Ag and Au), researchers are still mainly keen on synthesizing MO–Ag clusters. The insights into the cooperative effects of these MO–Ag clusters can trigger the directional design and controllable synthesis strategies of functional metal-oxo-modulated Cu or Ag metal cluster nanocomposites.

Conflicts of interest

There are no conflicts to declare.

Acknowledgements

This work is supported by the National Natural Science Foundation of China (22201038, 22101048, 21971038, 22271046 and 21975044), and the Fujian Provincial Department of Science and Technology (2019H6012, 21019L3004 and 2022J05040).

References

1 H. Huang, R. Shi, Z. Li, J. Zhao, C. Su and T. Zhang, Triphase photocatalytic CO_2 reduction over silver-decorated titanium oxide at a gas-water boundary, *Angew. Chem., Int. Ed.*, 2022, **61**, e202200802.
2 N. Zhang, X. Zhang, L. Tao, P. Jiang, C. Ye, R. Lin, Z. Huang, A. Li, D. Pang, H. Yan, Y. Wang, P. Xu, S. An, Q. Zhang, L. Liu, S. Du, X. Han, D. Wang and Y. Li, Silver single-atom catalyst for efficient electrochemical CO_2 reduction synthesized from thermal transformation and surface reconstruction, *Angew. Chem., Int. Ed.*, 2021, **60**, 6170–6176.
3 M. Yamamoto, T. Yoshida, N. Yamamoto, T. Nomoto, Y. Yamamoto, S. Yagi and H. Yoshida, Photocatalytic reduction of CO_2 with water promoted by Ag clusters in Ag/Ga_2O_3 photocatalysts, *J. Mater. Chem. A*, 2015, **3**, 16810–16816.
4 C. Hu, T. Peng, X. Hu, Y. Nie, X. Zhou, J. Qu and H. He, Plasmon-induced photodegradation of toxic pollutants with Ag-AgI/Al_2O_3 under visible-light irradiation, *J. Am. Chem. Soc.*, 2010, **132**, 857–862.
5 Y. Lei, F. Mehmood, S. Lee, J. Greeley, B. Lee, S. Seifert, R. E. Winans, J. W. Elam, R. J. Meyer, P. C. Redfern, D. Teschner, R. Schlogl, M. J. Pellin, L. A. Curtiss and S. Vajda, *Science*, 2010, **328**, 224–228.
6 L. Sun, K. Shen, H. Sheng, Y. Yun, Y. Song, D. Pan, Y. Du, H. Yu, M. Chen and M. Zhu, Au-Ag synergistic effect in CF_3-ketone alkynylation catalyzed by precise nanoclusters, *J. Catal.*, 2019, **378**, 220–225.
7 Y. Liu, X. Chai, X. Cai, M. Chen, R. Jin, W. Ding and Y. Zhu, Central doping of a foreign atom into the silver cluster for catalytic conversion of CO_2 toward C-C bond formation, *Angew. Chem., Int. Ed.*, 2018, **57**, 9775–9779.
8 Q. M. Wang, Y. M. Lin and K. G. Liu, Role of anions associated with the formation and properties of silver clusters, *Acc. Chem. Res.*, 2015, **48**, 1570–1579.
9 R. Ge, X.-X. Li and S.-T. Zheng, Recent advances in polyoxometalate-templated high-nuclear silver clusters, *Coord. Chem. Rev.*, 2021, **435**, 213787.
10 X. Fan, S. Chen, L. Zhang and J. Zhang, Protection of Ag clusters by metal-oxo modules, *Chem. – Eur. J.*, 2021, **27**, 15563–15570.
11 S. C. K. Hau, P.-S. Cheng and T. C. W. Mak, Ligand-induced assembly of coordination chains and columns containing high-nuclearity silver(I) ethynide cluster units, *Organometallics*, 2014, **33**, 3231–3234.
12 S. D. Bian, H. B. Wu and Q. M. Wang, A facile template approach to high-nuclearity silver(I) alkynyl clusters, *Angew. Chem., Int. Ed.*, 2009, **48**, 5363–5365.
13 K. Zhou, Y. Geng, L. K. Yan, X. L. Wang, X. C. Liu, G. G. Shan, K. Z. Shao, Z. M. Su and Y. N. Yu, An ultrastable

{$Ag_{55}Mo_6$} nanocluster with a Ag-centered multishell structure, *Chem. Commun.*, 2014, **50**, 11934–11937.

14 X. Y. Li, H. F. Su, M. Kurmoo, C. H. Tung, D. Sun and L. S. Zheng, Structure, solution assembly, and electroconductivity of nanosized argento-organic-cluster/framework templated by chromate, *Nanoscale*, 2017, **9**, 5305–5314.

15 Y. M. Su, W. Liu, Z. Wang, S. A. Wang, Y. A. Li, F. Yu, Q. Q. Zhao, X. P. Wang, C. H. Tung and D. Sun, Benzoate-induced high-nuclearity silver thiolate clusters, *Chem. – Eur. J.*, 2018, **24**, 4967–4972.

16 J. W. Liu, Z. Wang, Y. M. Chai, M. Kurmoo, Q. Q. Zhao, X. P. Wang, C. H. Tung and D. Sun, Core modulation of 70-nuclei core-shell silver nanoclusters, *Angew. Chem., Int. Ed.*, 2019, **58**, 6276–6279.

17 J. W. Liu, L. Feng, H. F. Su, Z. Wang, Q. Q. Zhao, X. P. Wang, C. H. Tung, D. Sun and L. S. Zheng, Anisotropic assembly of Ag_{52} and Ag_{76} nanoclusters, *J. Am. Chem. Soc.*, 2018, **140**, 1600–1603.

18 J. Qiao, K. Shi and Q. M. Wang, A giant silver alkynyl cage with sixty silver(I) ions clustered around polyoxometalate templates, *Angew. Chem., Int. Ed.*, 2010, **49**, 1765–1767.

19 X. Y. Li, Y. Z. Tan, K. Yu, X. P. Wang, Y. Q. Zhao, D. Sun and L. S. Zheng, Atom-precise polyoxometalate-Ag_2S core-shell nanoparticles, *Chem. – Asian J.*, 2015, **10**, 1295–1298.

20 G. G. Gao, P. S. Cheng and T. C. Mak, Acid-induced surface functionalization of polyoxometalate by enclosure in a polyhedral silver-alkynyl cage, *J. Am. Chem. Soc.*, 2009, **131**, 18257–18259.

21 X. Y. Li, Z. Wang, H. F. Su, S. Feng, M. Kurmoo, C. H. Tung, D. Sun and L. S. Zheng, Anion-templated nanosized silver clusters protected by mixed thiolate and diphosphine, *Nanoscale*, 2017, **9**, 3601–3608.

22 R. W. Huang, Q. Q. Xu, H. L. Lu, X. K. Guo, S. Q. Zang, G. G. Gao, M. S. Tang and T. C. Mak, Self-assembly of an unprecedented polyoxomolybdate anion $[Mo_{20}O_{66}]^{12-}$ in a giant peanut-like 62-core silver-thiolate nanocluster, *Nanoscale*, 2015, **7**, 7151–7154.

23 K. Zhou, C. Qin, H. B. Li, L. K. Yan, X. L. Wang, G. G. Shan, Z. M. Su, C. Xu and X. L. Wang, Assembly of a luminescent core-shell nanocluster featuring a $Ag_{34}S_{26}$ shell and a $[W_6O_{21}]^{6-}$ polyoxoanion core, *Chem. Commun.*, 2012, **48**, 5844–5846.

24 Z. Wang, H. F. Su, M. Kurmoo, C. H. Tung, D. Sun and L. S. Zheng, Trapping an octahedral Ag_6 kernel in a sevenfold symmetric Ag_{56} nanowhee, *Nat. Commun.*, 2018, **9**, 2094.

25 Z. Wang, H. F. Su, X. P. Wang, Q. Q. Zhao, C. H. Tung, D. Sun and L. S. Zheng, Johnson solids: anion-templated silver thiolate clusters capped by sulfonate, *Chem. – Eur. J.*, 2018, **24**, 1640–1650.

26 Z. Wang, H. Y. Zhuo, A. Y. Hu, H. F. Su, Q. Q. Zhao, X. P. Wang, C. H. Tung and D. Sun, Self-assembly of a novel Ag_{48} cluster encapsulating an unprecedented $[Mo_8O_{28}]^{8-}$ anion template, *Isr. J. Chem.*, 2018, **59**, 280–285.

27 H. Liu, C. Y. Song, R. W. Huang, Y. Zhang, H. Xu, M. J. Li, S. Q. Zang and G. G. Gao, Acid-base-triggered structural transformation of a polyoxometalate core inside a dodecahedrane-like silver thiolate shell, *Angew. Chem., Int. Ed.*, 2016, **55**, 3699–3703.

28 Z. Wang, H. F. Su, C. H. Tung, D. Sun and L. S. Zheng, Deciphering synergetic core-shell transformation from $[Mo_6O_{22}@Ag_{44}]$ to $[Mo_8O_{28}@Ag_{50}]$, *Nat. Commun.*, 2018, **9**, 4407.

29 D. E. Katsoulis, A survey of applications of polyoxometalates, *Chem. Rev.*, 1998, **98**, 359–388.

30 Z. G. Jiang, K. Shi, Y. M. Lin and Q. M. Wang, $[Ag_{70}(PW_9O_{34})_2(^tBuC{\equiv}C)_{44}(H_2O)_2]^{8+}$: ionothermal synthesis of a silver cluster encapsulating lacunary polyoxometalate ions, *Chem. Commun.*, 2014, **50**, 2353–2355.

31 B. J. Yan, X. S. Du, R. W. Huang, J. S. Yang, Z. Y. Wang, S. Q. Zang and T. C. W. Mak, Self-assembly of a stable silver thiolate nanocluster encapsulating a lacunary Keggin phosphotungstate anion, *Inorg. Chem.*, 2018, **57**, 4828–4832.

32 G. X. Duan, Y. P. Xie, J. L. Jin, L. P. Bao, X. Lu and T. C. W. Mak, High-nuclearity heterometallic tert-butylethynide clusters assembled with tert-butylphosphonate, *Chem. – Eur. J.*, 2018, **24**, 6762–6768.

33 Z. Wang, Y. J. Zhu, Y. Z. Li, G. L. Zhuang, K. P. Song, Z. Y. Gao, J. M. Dou, M. Kurmoo, C. H. Tung and D. Sun, Nuclearity enlargement from $[PW_9O_{34}@Ag_{51}]$ to $[(PW_9O_{34})_2@Ag_{72}]$ and 2D and 3D network formation driven by bipyridines, *Nat. Commun.*, 2022, **13**, 1802.

34 J. Y. Wang, K. G. Liu, Z. J. Guan, Z. A. Nan, Y. M. Lin and Q. M. Wang, $[Mn^{III}Mn^{IV}{}_2Mo_{14}O_{56}]^{17-}$: A mixed-valence meso-polyoxometalate anion encapsulated by a 64-nuclearity silver cluster, *Inorg. Chem.*, 2016, **55**, 6833–6835.

35 Y. Y. Li, F. Gao, J. E. Beves, Y. Z. Li and J. L. Zuo, A giant metallo-supramolecular cage encapsulating a single-molecule magnet, *Chem. Commun.*, 2013, **49**, 3658–3660.

36 S. S. Zhang, H. F. Su, Z. Wang, X. P. Wang, W. X. Chen, Q. Q. Zhao, C. H. Tung, D. Sun and L. S. Zheng, Elimination-fusion self-assembly of a nanometer-scale 72-Nucleus silver cluster caging a pair of $[EuW_{10}O_{36}]^{9-}$ polyoxometalates, *Chem. – Eur. J.*, 2018, **24**, 1998–2003.

37 S. S. Zhang, F. Alkan, H. F. Su, C. M. Aikens, C. H. Tung and D. Sun, $[Ag_{48}(^tBuC{\equiv}C)_{20}(CrO_4)_7]$: An atomically precise silver nanocluster co-protected by inorganic and organic ligands, *J. Am. Chem. Soc.*, 2019, **141**, 4460–4467.

38 G. X. Duan, J. Han, B. Z. Yang, Y. P. Xie and X. Lu, Oxometalate and phosphine ligand co-protected silver nanoclusters: $Ag_{28}(dppb)_6(MO_4)_4$ and $Ag_{32}(dppb)_{12}(MO_4)_4(NO_3)_4$, *Nanoscale*, 2020, **12**, 1617–1622.

39 F. Gruber and M. Jansen, $\{[Ag_{42}(CO_3)(^tBuC{\equiv}C)_{27}(CH_3CN)_2][CoW_{12}O_{40}]_2\}[BF_4]$: an intercluster sandwich compound, *Angew. Chem., Int. Ed.*, 2010, **49**, 4924–4926.

40 S. Tamari, K. Ono, M. Hashimoto and T. Ozeki, Control over the preference for binding sites of polyoxometalates to silver ethynide clusters by surface charge modification, *Dalton Trans.*, 2015, **44**, 19056–19058.

41 M. Kurasawa, F. Arisaka and T. Ozeki, Asymmetrically fused polyoxometalate-silver alkynide composite cluster, *Inorg. Chem.*, 2015, **54**, 1650–1654.
42 C. Zhan, J. M. Cameron, J. Gao, J. W. Purcell, D. L. Long and L. Cronin, Time-resolved assembly of cluster-in-cluster $\{Ag_{12}\}$-in-$\{W_{76}\}$ polyoxometalates under supramolecular control, *Angew. Chem., Int. Ed.*, 2014, **53**, 10362–10366.
43 Y. Kikukawa, Y. Kuroda, K. Yamaguchi and N. Mizuno, Diamond-shaped $[Ag_4]^{4+}$ cluster encapsulated by silicotungstate ligands: synthesis and catalysis of hydrolytic oxidation of silanes, *Angew. Chem., Int. Ed.*, 2012, **51**, 2434–2437.
44 Y. Kikukawa, Y. Kuroda, K. Suzuki, M. Hibino, K. Yamaguchi and N. Mizuno, A discrete octahedrally shaped $[Ag_6]^{4+}$ cluster encapsulated within silicotungstate ligands, *Chem. Commun.*, 2013, **49**, 376–378.
45 K. Yonesato, H. Ito, D. Yokogawa, K. Yamaguchi and K. Suzuki, An ultrastable, small $\{Ag_7\}^{5+}$ nanocluster within a triangular hollow polyoxometalate framework, *Angew. Chem., Int. Ed.*, 2020, **59**, 16361–16365.
46 K. Yonesato, H. Ito, H. Itakura, D. Yokogawa, T. Kikuchi, N. Mizuno, K. Yamaguchi and K. Suzuki, Controlled assembly synthesis of atomically precise ultrastable silver nanoclusters with polyoxometalates, *J. Am. Chem. Soc.*, 2019, **141**, 19550–19554.
47 K. Yonesato, S. Yamazoe, D. Yokogawa, K. Yamaguchi and K. Suzuki, A molecular hybrid of an atomically precise silver nanocluster and polyoxometalates for H_2 cleavage into protons and electrons, *Angew. Chem., Int. Ed.*, 2021, **60**, 16994–16998.
48 K. Yonesato, S. Yamazoe, S. Kikkawa, D. Yokogawa, K. Yamaguchi and K. Suzuki, Variable control of the electronic states of a silver nanocluster via protonation/deprotonation of polyoxometalate ligands, *Chem. Sci.*, 2022, **13**, 5557–5561.
49 Z. Wang, H. F. Su, L. P. Zhang, J. M. Dou, C. H. Tung, D. Sun and L. Zheng, Stepwise assembly of Ag_{42} nanocalices based on a Mo(VI)-anchored thiacalix[4]arene metalloligand, *ACS Nano*, 2022, **16**, 4500–4507.
50 Z. Wang, L. Li, L. Feng, Z. Y. Gao, C. H. Tung, L. S. Zheng and D. Sun, Solvent-controlled condensation of $[Mo_2O_5(PTC4A)_2]^{6-}$ metalloligand in stepwise assembly of hexagonal and rectangular Ag_{18} nanoclusters, *Angew. Chem., Int. Ed.*, 2022, **61**, e202200823.
51 M. Y. Gao, K. Wang, Y. Sun, D. Li, B. Q. Song, Y. H. Andaloussi, M. J. Zaworotko, J. Zhang and L. Zhang, Tetrahedral geometry induction of stable Ag-Ti nanoclusters by flexible trifurcate TiL_3 metalloligand, *J. Am. Chem. Soc.*, 2020, **142**, 12784–12790.
52 X.-M. Luo, C.-H. Gong, X.-Y. Dong, L. Zhang and S.-Q. Zang, Evolution of all-carboxylate-protected superatomic Ag clusters confined in Ti-organic cages, *Nano Res.*, 2020, **14**, 2309–2313.
53 S. Chen, W. H. Fang, L. Zhang and J. Zhang, Atomically precise multimetallic semiconductive nanoclusters with optical limiting effects, *Angew. Chem., Int. Ed.*, 2018, **57**, 11252–11256.
54 X. Fan, F. Yuan, D. Li, S. Chen, Z. Cheng, Z. Zhang, S. Xiang, S. Q. Zang, J. Zhang and L. Zhang, Threefold collaborative stabilization of Ag_{14} -nanorods by hydrophobic Ti_{16} -oxo clusters and alkynes: designable assembly and solid-state optical-limiting application, *Angew. Chem., Int. Ed.*, 2021, **60**, 12949–12954.
55 Y. M. Su, Z. Wang, G. L. Zhuang, Q. Q. Zhao, X. P. Wang, C. H. Tung and D. Sun, Unusual fcc-structured Ag_{10} kernels trapped in Ag_{70} nanoclusters, *Chem. Sci.*, 2019, **10**, 564–568.
56 Z. Wang, H. T. Sun, M. Kurmoo, Q. Y. Liu, G. L. Zhuang, Q. Q. Zhao, X. P. Wang, C. H. Tung and D. Sun, Carboxylic acid stimulated silver shell isomerism in a triple core-shell Ag_{84} nanocluster, *Chem. Sci.*, 2019, **10**, 4862–4867.
57 Q. Liu, S. He, B. Yu, X. Cheng, W. Shi and X. Wang, Visible light induced Ag–polyoxometalate coassembly into single-cluster nanowires, *Adv. Mater.*, 2022, e2206178.
58 J. Liu, W. Shi, B. Ni, Y. Yang, S. Li, J. Zhuang and X. Wang, Incorporation of clusters within inorganic materials through their addition during nucleation steps, *Nat. Chem.*, 2019, **11**, 839–845.
59 F. Gruber and M. Jansen, Supramolecular intercluster compounds consisting of 1D arrays of silver alkynyl clusters and Wells-Dawson Anions, displaying ligand-free interfaces, *Z. Anorg. Allg. Chem.*, 2011, **637**, 1676–1679.
60 A. Xie, Z. Wang, L.-P. Cheng, G.-G. Luo, Q.-Y. Liu and D. Sun, An extended AgI cluster-based framework solid: silver-thiolate cluster linked polyoxometalate including $Ag^I\cdots$H–C Anagostic Interactions, *Eur. J. Inorg. Chem.*, 2019, **2019**, 496–501.
61 Y. H. Li, Z. Y. Wang, B. Ma, H. Xu, S. Q. Zang and T. C. W. Mak, Self-assembly of thiolate-protected silver coordination polymers regulated by POMs, *Nanoscale*, 2020, **12**, 10944–10948.
62 Y. Xiao and Q. M. Wang, Luminescence responsive charge transfer intercluster crystals, *Chem. – Eur. J.*, 2012, **18**, 11184–11187.
63 X. Kang, X. Wei, S. Jin, S. Wang and M. Zhu, Controlling the crystallographic packing modes of Pt_1Ag_{28} nanoclusters: effects on the optical properties and nitrogen adsorption-desorption performances, *Inorg. Chem.*, 2021, **60**, 4198–4206.
64 Y. P. Xie and T. C. Mak, Silver(I)-ethynide clusters constructed with phosphonate-functionalized polyoxovanadates, *J. Am. Chem. Soc.*, 2011, **133**, 3760–3763.
65 Y. P. Xie and T. C. Mak, High-nuclearity silver ethynide clusters assembled with phosphonate and metavanadate precursors, *Angew. Chem., Int. Ed.*, 2012, **51**, 8783–8786.
66 Y. P. Xie and T. C. Mak, A pyrovanadate-templated silver(I)-ethynide cluster circumscribed by macrocyclic polyoxovanadate(V), *Chem. Commun.*, 2012, **48**, 1123–1125.
67 K. G. Liu, X. Y. Liu, Z. J. Guan, K. Shi, Y. M. Lin and Q. M. Wang, The transformation of polyoxometalates in the formation of intercluster compound $[Ag_{41}(\alpha\text{-}SiW_{10}O_{37})(^tBuC{\equiv}C)_{27}(CH_3CN)_3][\beta\text{-}SiW_{12}O_{40}]$, *Chem. Commun.*, 2016, **52**, 3801–3804.